Constraints on metasomatized mantle under Central South America: evidence from Jurassic alkaline lamprophyre dykes from the Eastern Cordillera, NM Argentina

Mineralogy and Petrology

ISSN 0930-0708
Volume 100
Combined 3-4

Miner Petrol (2010)
100:153-184
DOI 10.1007/
s00710-010-0127-5

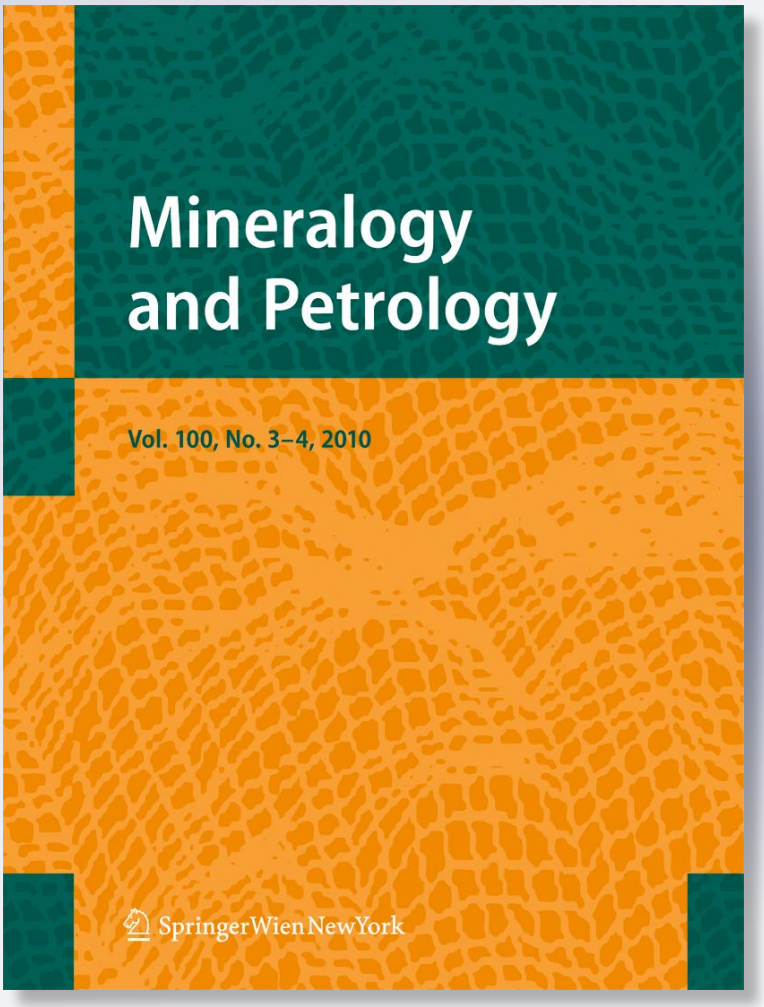

Springer

Miner Petrol (2010) 100:153–184
DOI 10.1007/s00710-010-0127-5

ORIGINAL PAPER

Constraints on metasomatized mantle under Central South America: evidence from Jurassic alkaline lamprophyre dykes from the Eastern Cordillera, NM Argentina

Natalia Hauser · Massimo Matteini · Ricardo H. Omarini · Márcio M. Pimentel

Received: 29 July 2008 / Accepted: 6 September 2010 / Published online: 25 September 2010

Abstract In the Río Grande Valley, NW Argentina, several porphyritic panidiomorphic, ocelli-bearing dykes and sills intrude the Neoproterozoic to lower Paleozoic basement of the Eastern Cordillera. New petrographical and geochemical data permit us to classify these rocks as ocellar-analcime monchiquites, a feldspar-free variety of alkaline lamprophyre composed of Ti-rich-diopside/augite, Ti-rich biotite/phlogopite, forsteritic olivine, titanian-pargasite and analcime, with abundant ocelli filled with analcime/carbonate. In terms of geochemical compositions they are characterized by LILE and LREE enrichment and lack of Nb-Ta and Eu anomalies. The $^{87}Sr/^{86}Sr$ and $^{143}Nd/^{144}Nd$ initial ratios range between 0.70377 to 0.70781 and 0.512506 and 0.512716 respectively, and T_{DM} model ages vary between 0.25–0.64 Ga. A K-Ar age of 163±9 Ma suggests that these rocks are related to the pre-rifting stage of the Mesozoic-Cenozoic continental Salta Rift in NW Argentina. Partial melting of a heterogeneous enriched metasomatized lithospheric mantle, magma mixing and fractionation are envisaged to explain the petrographic, geochemical and isotope characteristics of these magmas.

Editorial handling: K. R. Moore

N. Hauser · M. Matteini
Laboratório de Geocronologia, Instituto de Geociências,
Universidade de Brasília,
Brasília DF 70910-900, Brazil

N. Hauser (✉) · R. H. Omarini
Universidad Nacional de Salta-CONICET,
Buenos Aires 177,
Salta 4400, Argentina
e-mail: hausernatalia@yahoo.com.ar

M. M. Pimentel
Universidade Federal de Rio Grande do Sul (UFRGS),
Porto Alegre/RS 90040-060, Brazil

Introduction

During Mesozoic to Cenozoic times the whole of South America was affected by generalized extensional tectonics, related both to the subduction of the pacific oceanic plate beneath South America (Viramonte et al. 1999; Ramos 2000; Lucassen et al. 2007) and to the opening of the southern Atlantic Ocean (Sempere et al. 2002; Jacques 2003; Cristiani et al. 2005). In northwest Argentina the most prominent expression of this extensional tectonics was the Jurassic-Eocene continental Salta Rift that is typically characterized by a continental sedimentary sequence associated with bimodal magmatism (e.g. Viramonte et al. 1999; Menegatti 2001; Cristiani et al. 2005). This bimodal magmatism is represented by anatectic and mantle derived melts during the pre rift stage (Cristiani et al. 2005) whereas in the syn rift stage it is constituted by mantle derived basanitic and trachytic melts (Viramonte et al. 1999). The Salta Rift occupies a region between the Andean belt and the Brazilian cratonic area. The region could represent the transition between the metasomatised sub-arc mantle, generated during the various episode of subduction that occurred in Paleozoic times (Lucassen et al. 2005, 2007) and the old subcontinental mantle from the adjacent Brazilian shield.

In the Río Grande Valley (Jujuy province), several dykes and sills outcrop (Toselli and Aceñolaza 1984; Chayle and Coira 1987; Manca et al. 1987; Coira et al. 1990) spatially associated with the Tres Cruces branch of the Salta Rift (Fig. 1). These subvolcanic rocks intrude the

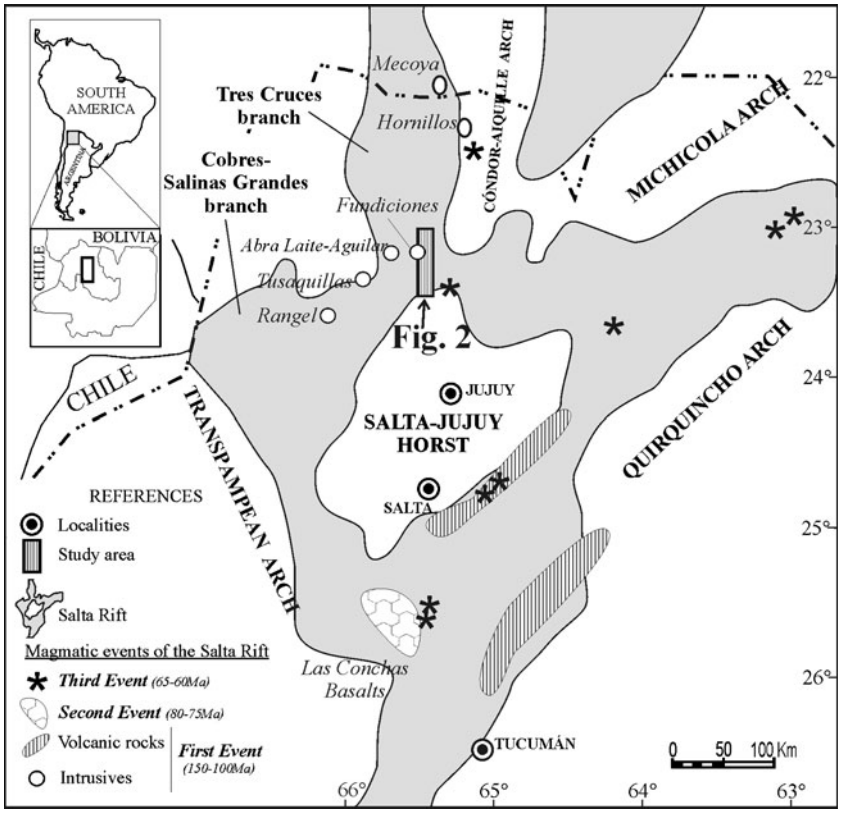

Fig. 1 Map of the syn-rift phase of the Jurassic-Cretaceous Salta Rift, NW Argentina. The location of pre-rift plutonic rocks and the study area are shown (modified from Salfity and Marquillas (1981) and Viramonte et al. (1999)

Neoproterozoic-Paleozoic sedimentary basement showing no apparent cross-cutting field relationships with the Cretaceous sediments related to the Salta rift. They were previously classified by several authors (Toselli and Aceñolaza 1984; Manca et al. 1987; Chayle and Coira 1987; Coira et al. 1990; Omarini et al. 1999), as ankaramites, pyroxenitic hornblendites, picrites and basalts with alkaline affinities, suggesting, on the basis of field evidence, a Neoproterozoic to Lower Paleozoic age. Nevertheless, due to the lack of detailed field and petrological data as well as of accurate geochronological data, it was not possible, until now, to characterize their ages, petrogenesis and the related tectonic settings.

This paper presents and discusses new field, petrographic, mineral chemical, geochemical, isotopic and geochronological data for subvolcanic rocks outcropping in the Río Grande Valley, Eastern Cordillera, NW Argentina. The data permitted to constrain the tectonic setting of emplacement, the petrogenesis of these magmas and the composition of the mantle under the Central Andes.

Geological and tectonic setting

Since the Early Mesozoic, the geodynamic evolution of the Andean margin has been characterized by a complex interaction between the Aluk-Phoenix, Farallon and Pacific oceanic plates and the South American continental plate (Zonenshayn et al. 1984; Scheuber et al. 1994; Jaillard et al. 2000). During the Lower Jurassic (Sinemurian-Pleinsbachian times) the subduction of the Aluk-Phoenix plate led to the development of a large magmatic arc along the western margin of South America, represented by subalkaline plutons and volcanic rocks (La Negra Formation) in northern Chile (Mpodoziz and Ramos 1990; Romeuf et al. 1995; Jaillard et al. 2000).

At the same time in southeastern Bolivia and northwestern Argentina, extensional tectonics began and continued until Eocene times with the formation and evolution of the continental Salta rift (Fig. 1), in a back-arc position relative to the Jurassic-Cretaceous volcanic arc (Salfity and Marquillas 1981; Avila Salinas 1986; Galliski and Viramonte 1988; Omarini et al. 1989). Important magmatic activity was associated with the Salta rift, including abundant alkaline-subalkaline plutonic and volcanic rocks (e.g. Galliski and Viramonte 1988; Rubiolo 1992; Viramonte et al. 1999; Menegatti 2001; Cristiani 2004; Comin-Chiaramonti et al. 2005; Cristiani et al. 2005). The extensional tectonics in NW Argentina has been related (Galliski and Viramonte 1988) to the subduction of the Aluk plate under South America and interpreted as an aborted foreland rift. Alternatively, Cristiani et al. (2005) associated the Upper Jurassic-Cretaceous magmatism in NW Argentina with the generalized extensional tectonics that affected South America during the break-up of Gondwana.

The Salta rift

The Salta rift represents an important lithospheric structure extending N-S for about 1000 km in NW Argentina and south Bolivia. It is constituted by interconnected grabens meeting at a triple junction and a central horst named Salta-Jujuy Horst (Fig. 1). The rift-related sedimentary sequence is represented by the Salta Group in NW Argentina (Moreno 1970; Reyes and Salfity 1973; Salfity and Marquillas 1981; Salfity 1982; Gomez Omil et al. 1989) and the Puca Group in Bolivia (Russo and Rodrigo 1965; Reyes and Salfity 1973; Cherroni 1977). The Salta Group comprises three main units: the Pirgua, the Balbuena and the Santa Bárbara subgroups.

During the evolution of the rift three major tectonic phases and three magmatic events have been recognized (Salfity and Marquillas 1981; Avila Salinas 1986; Galliski and Viramonte 1988; Omarini et al. 1989).

The Jurassic *pre-rift phase* (Fig. 1) is dominated by regional doming resulting from the rise of asthenospheric mantle, with associated crustal thinning and an intricate pattern of extensional faults (Salfity and Marquillas 1981; Galliski and Viramonte 1988). The pre-rift phase is characterized by anorogenic igneous complexes along the major NNE-striking tectonic structures. The oldest known magmatism that represents the *first magmatic event,* at ca. 150–100 Ma, (Viramonte et al. 1999) of the Salta Rift includes the Tusaquillas Plutonic Complex (152–145 Ma, Cristiani 2004), the Abra Laite-Aguilar intrusive complex (153 Ma, Cristiani et al. 2008), the Rangel Stock (142–127 Ma, Menegatti 2001), the Fundiciones pluton (Haschke et al. 2005) and Mecoya plutonic complex. This magmatism comprises mantle-derived basic to acid magmas and granitic anatectic melts that intruded the Late Precambrian/Lower Paleozoic metasedimentary sequences in NW Argentina (Lanfranco 1972; Rubiolo 1992; Menegatti 2001; Cristiani 2004).

The Cretaceous *syn-rift phase* (Fig. 1) is characterized by thermal subsidence, intracontinental rifting with related red bed infill, and marine ingressions recorded in the Pirgua Subgroup and Balbuena Subgroup respectively (Salfity and Marquillas 1981). *The second magmatic event (80–75 Ma)* occurred during this phase and comprises alkaline volcanism (basanites and mugearites) along the axis of the main tectonic structures of the Salta Rift (Galliski and Viramonte 1988; Omarini et al. 1989; Viramonte et al. 1999).

The Paleogene *post-rift stage* is represented by the fluvial-lacustrine sediments of the Santa Bárbara Subgroup. During this time, the *third igneous event (65–60 Ma)* occurred. It comprises basaltic sills intruded in the Pirgua Subgroup (Omarini et al. 1989) and basanites interbedded in the Balbuena and Santa Bárbara Subgroup in Argentina. Basanites, phonotephrites (Vargas Gil 1965; Galliski and Viramonte 1988) and basaltic lava flows (Castaño and Rodrigo 1978) associated with equivalent sedimentary successions are recorded in Bolivia.

The closure, uplift and erosion of the Cretaceous-Paleocene rift basin occurred mainly in the late Eocene-early Oligocene during the Incaic orogeny (Sempere et al. 2002) which represents one of the major tectonic phases in the Central Andes.

Mafic and ultrabasic dykes in NW Argentina

In the north of Argentina and in southeastern Bolivia, subvolcanic alkaline rocks of different ages outcrop. In the Subandean belt, approximately 100 km east of the Río Grande Valley in Argentina, ultramafic alnoitic dykes have been dated at 303±10 Ma (K-Ar ages: Mendez and Villar 1979; Barbieri et al. 1997). In north Argentina, close to the Bolivian border, in the Santa Victoria Sierra, ultramafic lamprophyre ailikitic dykes with 224±08 Ma (K-Ar) ages were reported (Rubiolo et al. 1997).

Further to the south sannaites associated with the Upper Cretaceous Hornillos alkaline complex, which intruded into the Neoproterozoic-Lower Paleozoic basement rocks, are recorded (Rubiolo et al. 1997). These rocks are interpreted to represent igneous activity associated with extensional processes during the formation of the intracontinental Salta rift (Galliski and Viramonte 1988; Rubiolo 1992; Rubiolo et al. 1994; Rubiolo et al. 1997). Two lamprophyre dykes in this complex gave K-Ar ages of 71±9 and 59±4 Ma (Rubiolo et al. 2003).

Local geology

The study area is located in the Jujuy Province between 23º 35′ 00.01″ and 23º 09′ 13.00″ S of latitude and 65º 27′ 27.00″ and 65º 22′ 00.01″ W of longitude (Figs. 1 and 2). The oldest unit outcropping in the area is the Puncoviscana Formation (Turner 1960), made up of intensively folded turbidites consisting of alternating centimetric to decimetric beds of greywackes and pelites. During late Neoproterozoic to early Cambrian times an important deformational event, known as the Tilcaric Orogeny (Turner and Mendez 1975), occurred in NW Argentina. As a result, the sedimentary sequence of the Puncoviscana Formation was intensely folded. This unit is unconformably overlain by pink sandstones of the Middle to Upper Cambrian Meson Group that is interpreted as a shallow-marine passive margin system (Kumpa and Sanchez 1988). The greywackes and pelites of the Ordovician Santa Victoria Group of the Famatinian Cycle (Turner 1960; Bahlburg 1998 and references therein) overlie the Meson Group with a transitional contact. In Caradoc times the Ocloyic diastrophic phase

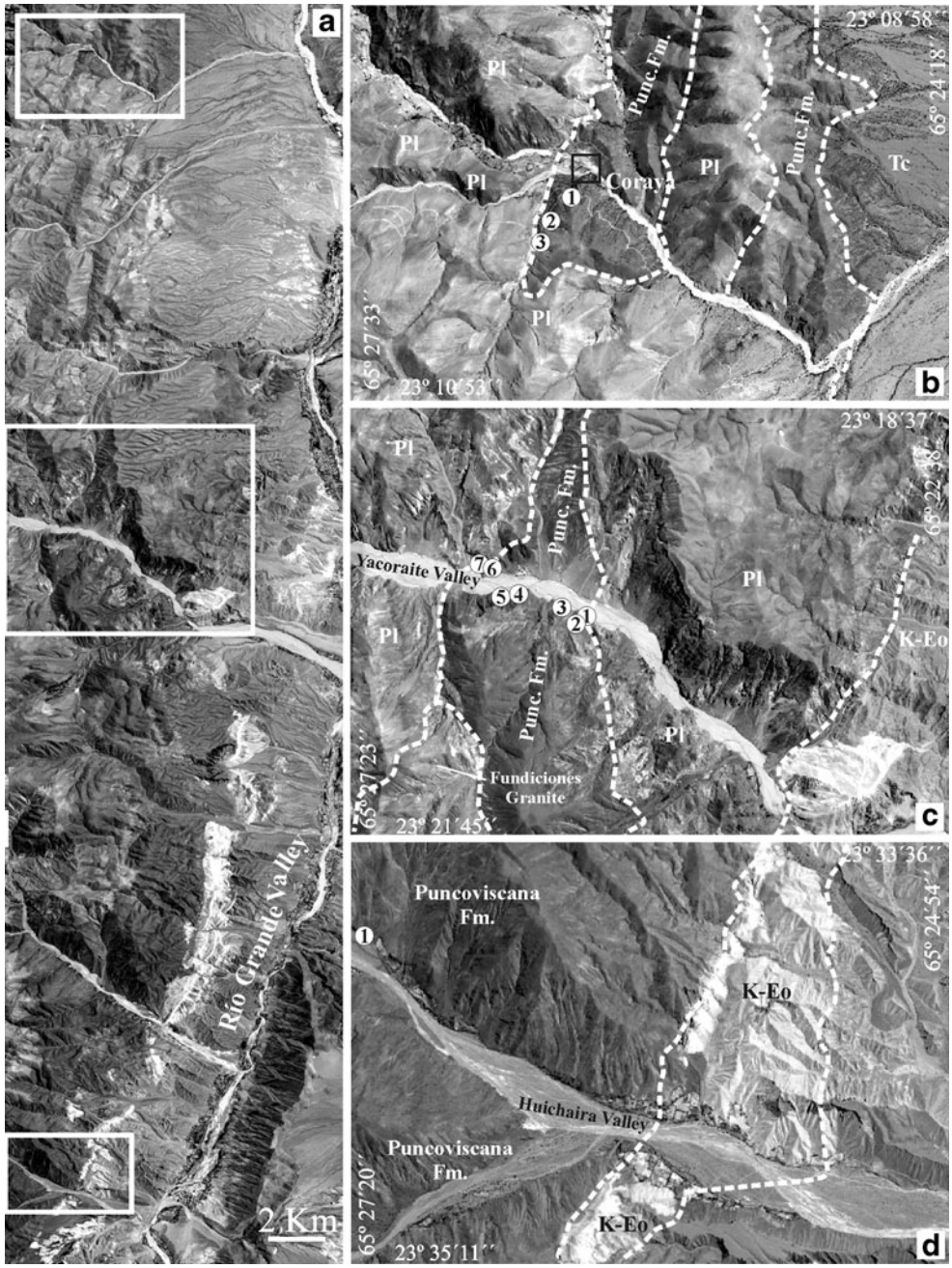

Fig. 2 **a** Geological sketch map on the of the Río Grande area (from http://www.google.com/earth/index.html). Detailed satellite images of Coraya ocality, Yacoraite Valley and Huichaira Valley with the outcrops and position of studied rocks: **b** from Coraya locality, 1-BCO 49, 2- BCO 51 and 3-BCO 52. **c** from Yacoraite Valley, **1**-BYA 122, **2**- BYA 123, **3**-BYA 124a-b, **4**- BYA 125, **5**- BYA 126, **6**- BYA 127, **7**- P8 and **d** from Huichaira Valley, 1-BHU 131. Symbols: Punc. Fm.: Puncoviscana Formation. Pl: Mesón and Santa Victoria Early Palaeozoic Groups. K-Eo: Salta Group. Tc: Tertiary

(Mon 1993) generated important thrust tectonics in this region (Seggiaro and Gallardo 2002).

The folded Neoproterozoic-Palaeozoic sedimentary basement is overlain by the Cretaceous-Tertiary sediments of the Salta Group, the latter is constituted by the red-beds of the Pirgua Subgroup and sandstones, limestones and evaporites of the Balbuena Subgroup. South of the Yacoraite Valley, the Jurassic Fundiciones granite (Haschke et al. 2005) which is linked with the pre-rift magmatic phase intruded the Palaeozoic basement. After the deposition of the Salta Group, the Andean thrust tectonics reactivated the ancient Salta rift faults generating faults with detachments that involved large thickness of the Neoproterozoic-Palaeozoic sedimentary basement. In Fig. 3, a schematic stratigraphic column of the sequences that outcrop in the Río Grande Valley is shown.

Several dykes and sills, which are the object of this study, outcrop in the Coraya (Toselli and Aceñolaza 1984), Yacoraite (Chayle and Coira 1987; Manca et al. 1987; Coira et al. 1990) and Huichaira secondary valleys (Hauser et al. 2008) and intrude the sediments of Puncoviscana Fm. (Figs. 2 and 3). Coira et al. (1990) also identified dykes and sills intruding Mesón and Santa Victoria Groups in the Yacoraite Valley. They are characterized by thickness varying from a few centimeters up to 50–60 cm. They are

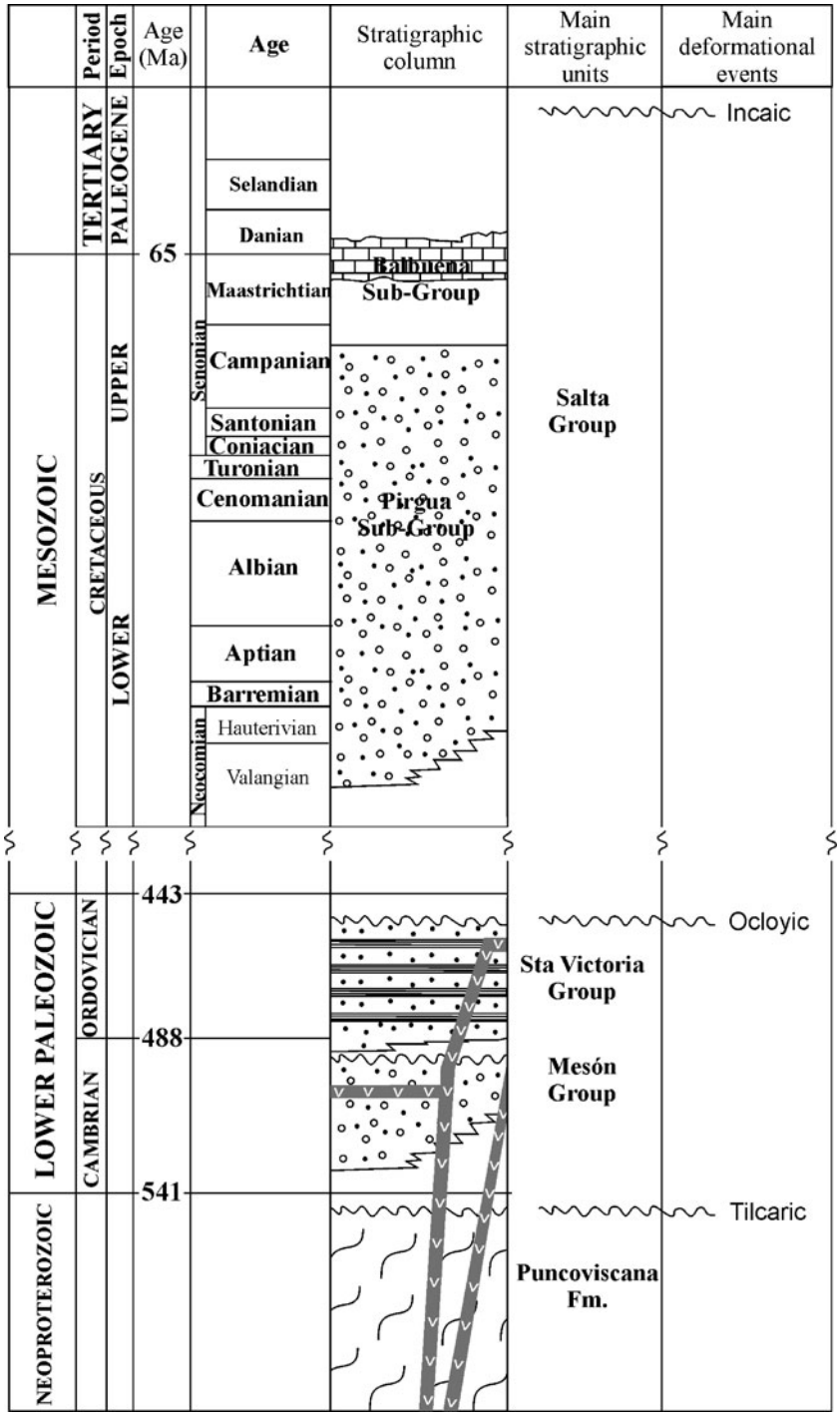

Fig. 3 Schematical stratigraphic column of the Río Grande Valley. The studied subvolcanic rocks in the Neoproterozoic-Early Palaeozoic basement rocks occur as sill-like to dike-like intrusions

generally folded, showing complex geometric relationships with the sedimentary host rock varying from sill-like to dyke-like intrusions (Fig. 4).

The Río Grande dykes and sills and sampling

The best exposures of these tabular intrusions are found in the Yacoraite Valley, where approximately 15–20 sills and dykes outcrop (Figs. 2 and 4). Two varieties of subvolcanic rocks have been identified in this study on the basis of mineralogy and textures: (i) dykes and sills characterized by aphanitic to porphyritic textures with clinopyroxene phenocrysts (Fig. 4a), and (ii) dykes characterized by highly porphyritic textures with mica and amphibole macrocrysts up to 2 cm. This type contains abundant xenoliths (Fig. 4b, c) concentrated along preferential zones, (e.g. sample P8), probably indicating flow differentiation. Almost all dykes show well developed, 5–10 cm thick, fine-grained chilled

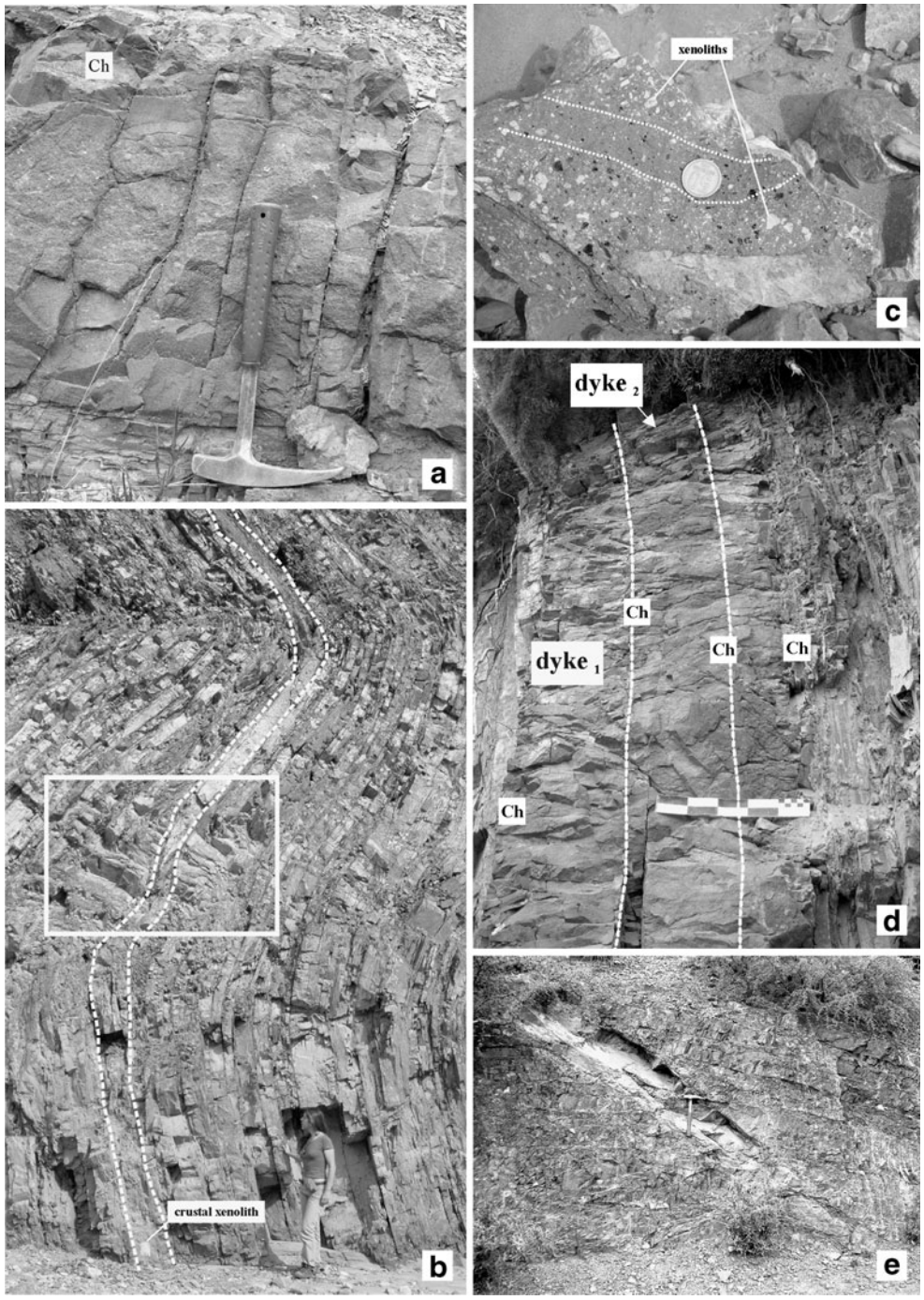

Fig. 4 Field features of the Río Grande dykes and sills. **a** Typical aspect of sample BYA 123 tabular intrusion displaying well developed chilled margins (Ch). **b** Sample BYA 126 tabular intrusion, intruding a pre-existing fold in the Puncoviscana Formation and showing locally cross-cutting relations (inset), **c** flow differentiation of mica, amphibole and xenoliths are shown by the this sample. **d** Example of dyke-in-dyke intrusion for sample BYA 124 tabular intrusion. The dyke$_2$ intrudes dyke$_1$ developing mm-size chilled margins (Ch). Scalebar is 25 cm long. e) Aspect of sample BCO 52 dyke intruding the Puncoviscana Formation in the Coraya locality

margins, and caused a local thermal metamorphism and bleaching of the host pelites (Fig. 4a). This suggests that a volatile rich melt was emplaced into a relatively cool basement at upper- to medium- crustal levels (Delor and Rock 1991).

The dyke of sample BYA 124a (Fig. 4d), has a thickness of about 50 cm and is characterized by a fine-grained to medium-grained porphyritic texture and aphanitic chilled margins of ~1 cm at the contact with the sedimentary host. This dyke is intruded in the central part by a younger dyke (of sample BYA 124b), with the same texture and mineralogical composition, that exhibits two thin (less than 0.5 cm) aphanitic chilled margins. These characteristics indicate a multiple dyke-in-dyke injection, a typical feature associated with extensional settings. A total of seven dyke-like to sill-like intrusions and sills from Yacoraite Valley (Fig. 2) were selected on the basis of field, lithological and petrographic characteristics (Table 1). They are the best preserved intrusive bodies and represent the two textural varieties recognized in the valley.

In the Coraya Valley, more than ten dykes and sills were recognized. These tabular intrusions (Fig. 4e) have thickness less than 30 cm, show fine-grained borders, and contain small dark fragments of thermometamorphosed host pelites. The dykes and sills are characterized by porphyritic textures with euhedral olivine and pyroxene phenocrysts, partially replaced by pseudomorphic calcite. The three best preserved tabular intrusions of the Coraya locality were selected for this study. They have different types of relationships with the basement rocks (see Table 1).

In the Huichaira Valley, the sedimentary sequence is strongly fractured, which makes it difficult to correlate different outcrops and hinders the characterization of individual dykes. Three main dykes were identified in this valley but samples of only the best preserved body (Table 1) were collected. They show fine-grained margins and columnar jointing, and are characterized by porphyritic texture with altered olivine phenocrysts.

Petrography

The *Yacoraite and Huichaira Valleys* lamprophyres have porphyritic to seriate, panidiomorphic textures, globular structures and xenoliths of both crustal and mantle origin. On the basis of the main mineralogy, two groups of rocks are recognized: an *olivine-bearing amphibole-free group* and an *olivine-free amphibole-bearing group.*

The first group, represented by samples BYA 122, 123, BYA 124, BYA 127 from the Yacoraite Valley and BHU 131 from Huichaira Valley (Table 1), is characterized by the presence of Ti-rich zoned clinopyroxene and olivine phenocrysts (Fig. 5a) and the lack of amphibole. Samples BYA 127 and BHU 131 show abundant olivine phenocrysts (Fig. 5b) whereas samples BYA 122, BYA 123 and BYA 124 exhibit predominantly clinopyroxene phenocrysts. In both cases the phenocrysts represent 10–30% of the rock and are hosted in an aphanitic groundmass constituted by prismatic microcrysts of clinopyroxene, abundant mica and carbonate/analcime (Fig. 5b). Globular structures of carbonate and analcime are common (Fig. 5i, j). In this group, poikilitic phenocrysts of clinopyroxene with olivine inclusions occur (Fig. 5g).

The second group is represented by samples P8 and BYA 126 (Table 1), from the Yacoraite Valley. This group is characterized by zoned amphibole, clinopyroxene and phlogopite phenocrysts together with apatite microphenocrysts (Fig. 5c, d). The groundmass is made of carbonate enclosing abundant microliths of biotite, amphibole and apatite (Fig. 5d). In sample P8, two types of clinopyroxene are present: the first named as *green core clinopyroxene* are euhedral to subhedral crystals, with green cores, pale pink rims, often surrounded by analcime; the second type is *colourless clinopyroxene* that forms anhedral to subhedral crystals. Similarly, two distinct varieties of amphibole phenocrysts are recognized (Fig. 5d). One variety is named *brown core amphiboles* and shows zoning from a brown core to pale brown rims; the other variety is named *green core amphiboles* and shows zoning from a green core to pale brown rims. Phlogopite phenocrysts exhibit strong zoning with dark brown core and pale brown rims. Clinopyroxene macrocrysts with apatite inclusions (Fig. 5h) ranging from 0.5 to 1 mm are common (Table 2).

Cognate lithics (Fig. 5e) and crustal xenoliths are common in this second group. The cognate lithics are composed of hornblende, clinopyroxene and phlogopite with petrographic features similar to the phenocrysts. The crustal xenoliths are chiefly hornblendite and are rounded to subangular and 2–60 mm in size. They consist mainly of brown unzoned amphibole and minor brown biotite and clinopyroxene showing crystalloblastic polygonal textures. Rare clinopyroxene-bearing carbonatite-like xenoliths are present (Fig. 5f). They are small (5 mm in diameter) and dolomite-rich, with minor clinopyroxene and Fe-Ti oxide crystals. Triple junctions between crystals of clinopyroxene and carbonate are observed. Macrocrysts formed by brown amphibole included poikilitically by olivine or diopside crystals were recognized (not shown).

The *Coraya Valley* rocks have a porphyritic, panidiomorphic texture with phenocrysts of olivine and pyroxene with pseudo-hexagonal and pseudo-octagonal outlines, which are completely replaced by calcite and serpentine. The phenocrysts make up approximately 25% of the rock. The aphanitic groundmass is extensively altered to carbonate and is characterized by the presence of abundant biotite and minor Fe-Ti oxide crystals. These latter phases also occur as poikilitic inclusions in the rims of olivine and pyroxene phenocrysts.

Globular structures

A characteristic feature of the Río Grande subvolcanic rocks is the presence of ocelli and segregation textures, extensively described in the literature as a common feature in alkaline lamprophyres (Fareeduddin et al. 2001; Azbej et al. 2006; Nedli and Tóth 2007). The ocelli show globular shapes, display rounded to elongated forms and are approximately 1.0 mm in diameter. Segregations (Rock 1979, 1991), i.e. leucocratic structures with no clear limits and gradation into their hosts, are observed.

On the basis of their mineral compositions, three types of ocelli have been recognized: (i) *Type-I ocelli,* the least abundant type, have globular to elongated carbonate cores surrounded by radial clinopyroxene and some acicular apatite crystals. The contact with their host is generally sharp (for example, in sample BHU 131, Fig. 5i). (ii) *Type-II ocelli* (Fig. 5j) are more abundant and are characterized by

Table 1 Summarized lithological and petrographic characteristics of the Río Grande sills and dykes

Locality	Sample N°	Relationships	Host rock	Texture	Alteration	Phenocrysts	Groundmass	Ocelli	Mantle xenoliths
Coraya	BCO 49	sill-like dyke-like, 30 cm thicks	Turbidites of Puncoviscana Formation	porphyritic- strongly panidiomorphic	Altered	Ol, Cpx (altered to carbonate, Serp)	Abundant Fe-ti oxides, Cpx, Bio	Scarce. Carbonate compositions	Not observed
	BCO 51	sill, 40 cm thick			Altered				
	BCO 52	dyke, 50 cm thick			Altered				
Yacoraite	P8	sill-like to dyke-like intrusion	Turbidites of Puncoviscana Formation	porphyritic; panidiomorphic, flow differentation	Fresh	Amph, Bio, Cpx, Ap	Amph, Cpx, Phlog, Apatite, Analcima, Carbonate, Fe-Ti oxides	Scarce. Carbonate compositions	Abundant, 0.5–5 cm large. Carbonatitic and amphibolitic compositions
	BYA 122	sill		porphyritic	Altered	Cpx completly altered to carbonate	Carbonate, Fe-Ti oxides	Not observed	Not observed
	BYA 123	sill		porphyritic, panidiomorphic, crystals rich	Slitghly altered	Cpx, scarce Ol altered to talc	Cpx, Bio, Fe-Ti oxides	Scarce. Carbonate-analcime compositions	Not observed
	BYA 124	sill-like to dyke-like multiple intrusions		porphyritic, panidiomorphic, crystals rich	Fresh	Strongly zoned titanian Cpx, Bio, scarce Ol	Cpx, Bio, Fe-Ti oxides	Scarce. Carbonate compositions	Not observed
	BYA 125	sill-like to dyke-like		porphyritic	Strongly altered	Not observed. Completely altered to Fe-Ti oxides	Not observed. Completely altered to Fe-Ti oxides	Not observed	Not observed
	BYA 126	sill-like to dyke-like		porphyritic, panidiomorphic	Altered	Amph, Cpx, Bio	Amph, Bio	Not observed	Abundant. Amphibolitc compositions
	BYA 127	sill-like to dyke-like		porphyritic, panidiomorphic, cpx glomeroporphyritic	Fresh	Ol, Cpx	Cpx, Bio, Fe-Ti oxides	Abundant. Carbonate compositions	Not observed
Huichaira	BHU 131	sill-like to dyke-like	Turbidites of Puncoviscana Formation	porphyritic-panidiomorphic-glomeroporphyritic	Slitghly altered	Cpx, Ol (altered to carbonate and talc), Bio	Bio, Fe-Ti oxides	Abundant. Carbonate-analcime, carbonate and cpx compositions. Segregations	Not observed

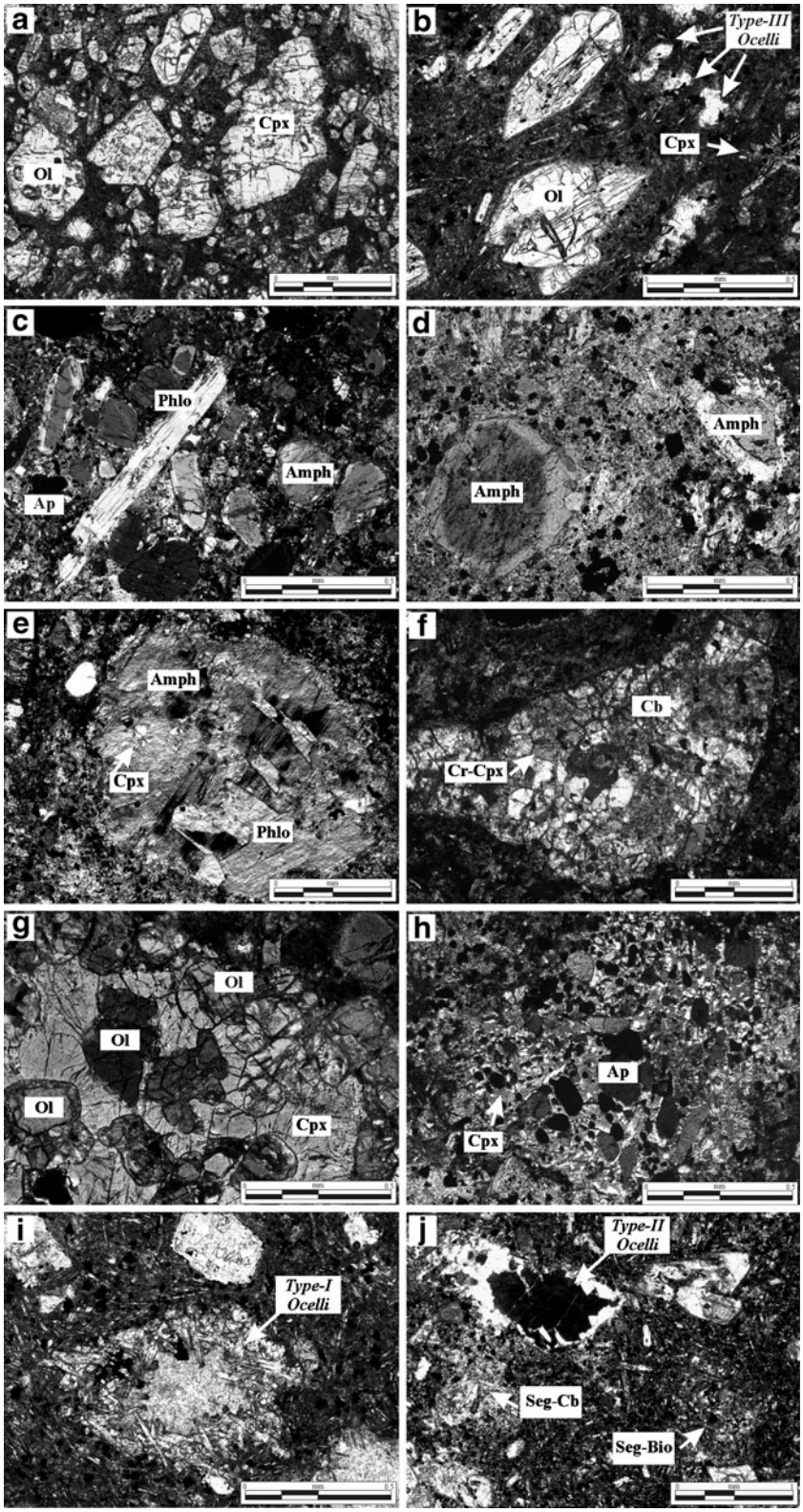

Fig. 5 Photomicrographs of typical features exhibited by the Río Grande subvolcanic rocks: *Olivine-bearing amphibole-free group*: **a** porphyritic texture with euhedral, zoned clinopyroxene (Cpx) and minor euhedral altered olivine (Ol) phenocrysts. Note the high crystals/groundmass proportions and **b** euhedral olivine phenocrysts in the groundmass. These commonly show instable features as embayment. The groundmass is composed by abundant clinopyroxene and biotite crystals. In this photomicrograph is observed also the *Type-III ocelli*, completely formed by carbonate. *Amphibole -bearing olivine -free group:* **c** typical porphyritic texture of sample P8 with abundant zoned amphibole (Amph) and zoned phlogopite (Phlo) phenocrysts, and apatite (Ap) microphenocryst (extinct position) and **d** two amphibole types, the brown-core and the green-core varieties (sample P8). Note the high carbonate and mica concentrations in the groundmass. The green core amphibole has a rim of Ba- and Sr-rich carbonate. **e** Cognate lithic in sample P8, composed by amphiboles, clinopyroxenes and phlogopites. **f** Clinopyroxene bearing carbonatite-like xenolith from sample P8, constituted by Ba- and Sr-rich carbonate (Cb), and minor Cr-rich augite (Cr-Cpx). **g** Phenocryst of poykilitic diopside (Cpx) with inclusion of olivine crystals (Ol) from sample BYA 123 of the *Olivine-bearing amphibole-free group*. **h** Phenocryst of poikilitic augite enclosing abundant apatite (Ap) crystals (extinct position) in the *Amphibole -bearing olivine -free group*. **i** Characteristics of *Type-I ocelli*: concentric zones of carbonate surrounded by radial diopside crystals. **j** The *Type-II ocelli* and segregations. This ocelli type is marked by analcime forming the central pool surrounded by carbonate. The segregations are characterized by high concentrations of biotite microphenocrysts (Seg-Bio) or by high concentrations of carbonate (Seg-Cb)

analcime surrounded by carbonate crystals. Occasionally biotite crystals occur at the rim or inside the ocelli. The contact between this type of ocelli and the host groundmass is marked by carbonate-rich and biotite-poor segregations. The *Type-III ocelli* (Fig. 5b) are very common and composed of carbonate, occasionally surrounded by biotite or Ti-Fe oxide.

Two compositional end members of segregations are identified according to the proportion of carbonate or Ti-rich

Table 2 Representative modal abundances (%) of alkaline lamprophyres from Río Grande Valley

	P8	BYA 123	BYA 124	BYA 127	BYA 131
Phenocrysts					
Olivine	0	4	10	21	20
Clinopyroxene	7	39	41	4	9
Amphibole	22	0	0	0	0
Bio/Phlogopite	12	2	0	0	0
Apatite	2	0	0	0	0
Lithics	12	< 1	1	0	0
Groundmass					
Analcime	7	4	3	12	14
Carbonate	13	4	3	7	6
Clinopyroxene	0	13	14	23	20
Amphibole	7	0	0	0	0
Bio/Phlogopite	11	30	22	27	25
Apatite	1	0	0	0	0
Opaques	6	4	6	6	6
TOTAL	100	100	100	100	100

biotite: a Ti-biotite rich and carbonate poor type (Seg-Bio in Fig. 5j), and a carbonate rich and Ti-biotite-poor type (Seg-Cb in Fig. 5j). The second type is commonly in contact with the *Type-II ocelli*.

Petrographic characteristics such as the presence of (i) porphyritic panidiomorphic textures, (ii) leucocratic carbonate-analcime rich ocelli and (iii) abundance of hydrated minerals such as amphibole and phlogopite, permitted us to classify the Río Grande subvolcanic rocks as alkaline lamprophyres.

Mineral chemistry

The composition of minerals was obtained using a CAMECABAX SX 50 electron microprobe at the Electron Microprobe Laboratory of the University of Brasilia (Brazil). Wavelength-Dispersive (WDS) analyses were performed at an accelerating voltage of 15 kV and a beam current of 25 nA with a spot size of 1 μm. Acquisition time was 100 s. Each element was standardized using either synthetic or natural minerals. Mineral chemistry studies were carried out for olivine, clinopyroxene, amphibole, mica, analcime, apatite and carbonates from the better preserved dykes of the Yacoraite and Huichaira Valleys.

Olivine

Representative compositions of olivine of samples BYA 124a and BYA 127 from the Yacoraite Valley are shown in Table 3. Compositions of olivine phenocrysts as well as xenoliths range from Fo_{76} to Fo_{86}. Phenocrysts in sample BYA 127 show a slight decrease in forsterite content from cores (Fo_{86}) to rims (Fo_{84}) but in general, all phenocrysts, microphenocrysts and xenolith crystals have rather homogeneous compositions (limited intra-grain variation).

Clinopyroxene

The compositions of clinopyroxene are shown in Tables 4 and 5; they represent phenocrysts/microphenocrysts, groundmass microliths, as well as crystals in hornblendite and clinopyroxene-bearing carbonatite-like xenoliths. According to the nomenclature proposed by Morimoto et al. (1988), all the analyzed crystals belong to the calcic series.

Most of the clinopyroxenes fall in the Fe-diopside field, with some macrocrysts and crystals from clinopyroxene-bearing carbonatite-like xenoliths falling in the Mg-augite field. In all samples an evolution trend toward salite composition is observed (Fig. 6).

In sample P8 the *green core clinopyroxenes* have cores with high Na_2O content (~2.5 wt. %) and Mg# of ~67, and shows reverse zoning, with rims having lower Na_2O (<1 wt. % of Na_2O) and higher Mg# ~74, whereas the *colourless clinopyroxenes* have cores with less Na_2O (~1.3 wt. %), higher Mg# of ~78 (Table 5), and normal zoning with rims showing Na_2O <0.9 wt. % and lower Mg# of ~74. In the clinopyroxene-bearing carbonatite-like xenoliths from the same sample, augite crystals are classified as chromian-sodian augite with high Cr_2O_3 content (up 1.1 wt. %) and Mg# of ~90 (Table 5).

Clinopyroxenes from samples BYA 123, 124a, 127 and BHU 131 have increasing Ti content from core to rim, with some crystal rims being titanian-diopside (> 0.10 Ti apfu). In the Al_2O_3/Mg# vs. TiO_2 diagram (Fig. 7) two groups with different compositions are observed. The first group composed of clinopyroxene crystals from samples BYA 127 and BHU 131 displays a positive trend with higher TiO_2 contents. The second group represented by clinopyroxenes from sample P8 shows a similar trend but with lower TiO_2 contents. Clinopyroxenes of samples BYA 123 and BYA 124 are intermediate in composition between the two groups. Three clinopyroxenes from *Type-I ocelli* in sample BYA 127 show distinctive compositions with low Al_2O_3/Mg# and TiO_2 contents. The clinopyroxenes from cognate lithics (sample P8) show the lowest Al_2O_3/Mg# and TiO_2 contents whereas the clinopyroxenes from the carbonatite-like xenoliths (sample P8) are characterized by low TiO_2 and intermediate Al_2O_3/Mg# values.

Amphibole

Amphibole, present in samples P8 and BYA 126, has been analyzed only in sample P8 that shows the best preserved minerals. The analyses on sample P8 were carried out on

Table 3 Representative electron microprobe analyses of olivine minerals of the Río Grande subvolcanic rocks

	BYA 127												BYA 124a		
	Phenocrysts											Mesophenocrysts	Phenocrysts		in poikilitic cpx phenocryst
	1			2			3			4		5	6	7	8
	Rim	Inter	Core	Rim	Inter	Core	Rim	Inter	Core	Rim	Core				
SiO_2	40.32	40.21	40.22	39.47	39.59	39.66	39.52	38.87	39.38	39.52	39.64	40.42	39.49	38.06	39.60
TiO_2	0.05	0.01	0.02	0.07	0.01	0.01	0.00	0.03	0.05	0.06	0.07	0.03	0.02	0.03	0.03
Al_2O_3	0.08	0.02	0.05	0.01	0.03	0.05	0.02	0.03	0.06	0.03	0.02	0.03	0.01	0.02	0.07
$FeO_{(t)}$	15.00	13.05	13.20	15.08	14.11	13.10	15.03	18.94	19.14	14.84	13.40	14.97	17.04	21.96	14.28
MnO	0.22	0.15	0.18	0.25	0.12	0.12	0.26	0.24	0.24	0.27	0.12	0.18	0.22	0.31	0.19
MgO	44.02	45.56	45.21	44.12	44.79	45.68	43.70	41.14	41.16	44.16	44.88	44.36	42.86	39.05	44.50
CaO	0.42	0.21	0.24	0.40	0.26	0.23	0.38	0.15	0.11	0.43	0.22	0.33	0.31	0.13	0.21
Cr_2O_3	0.08	0.04	0.03	0.09	0.04	0.07	0.05	0.03	0.01	0.09	0.01	0.00	0.01	0.01	0.03
NiO	0.19	0.32	0.31	0.15	0.21	0.20	0.20	0.21	0.16	0.15	0.20	0.24	0.29	0.18	0.30
K_2O	0.00	0.01	0.01	0.00	0.01	0.01	0.01	0.01	0.00	0.00	0.00	0.01	0.01	0.00	0.00
Total	100.38	99.58	99.46	99.63	99.17	99.13	99.16	99.64	100.30	99.53	98.56	100.56	100.25	99.75	99.20
Cations															
Si	1.01	1.01	1.01	1.00	1.00	1.00	0.01	0.00	0.00	0.00	0.01	0.01	0.01	0.00	0.00
Ti	0.00	0.00	0.00	0.01	0.01	0.01	1.65	1.58	1.57	1.66	1.69	1.65	1.62	1.52	1.68
Al	0.00	0.00	0.00	0.00	0.00	0.00	0.00	0.00	0.00	0.00	0.00	0.00	0.00	0.00	0.00
Fe	0.31	0.27	0.28	0.32	0.30	0.28	0.32	0.41	0.41	0.31	0.28	0.31	0.36	0.48	0.30
Mn	0.01	0.00	0.00	0.01	0.00	0.00	1.00	1.00	1.01	1.00	1.00	1.01	1.00	0.99	1.00
Mg	1.64	1.70	1.69	1.66	1.69	1.71	0.00	0.00	0.00	0.00	0.00	0.00	0.00	0.00	0.00
Ca	0.01	0.01	0.01	0.00	0.00	0.00	0.01	0.01	0.01	0.01	0.00	0.00	0.01	0.01	0.00
Cr	0.00	0.00	0.00	0.00	0.00	0.00	0.00	0.00	0.00	0.00	0.00	0.00	0.00	0.00	0.01
Ni	0.00	0.01	0.01	0.00	0.00	0.00	0.00	0.00	0.00	0.01	0.00	0.00	0.00	0.00	0.01
K	0.00	0.00	0.00	0.00	0.00	0.00	0.00	0.00	0.00	0.00	0.00	0.01	0.01	0.00	0.00
TOTAL	2.99	3.00	2.99	3.00	3.00	3.00	3.00	3.00	2.99	3.00	3.00	2.99	3.00	3.01	3.00
Fo	84.24	86.27	86.04	84.14	85.18	86.30	84.03	79.44	79.22	84.39	85.80	84.30	81.92	75.89	84.82
Fa	16.11	13.86	14.10	16.13	15.05	13.88	16.21	20.52	20.67	15.91	14.37	15.95	18.28	23.94	15.27
Mg#*	0.75	0.78	0.77	0.75	0.76	0.78	0.74	0.68	0.68	0.75	0.77	0.75	0.72	0.64	0.76

*Mg#=Mg/(Mg+Fetot)

Table 4 Representative electron microprobe analyses of clinopyroxene minerals of the Río Grande subvolcanic rocks

	BYA 123			BYA 124				BYA 127			BHU 131								
	Phenocrysts			Phenocrysts			Poikilitic cpx with ol inclusion	Mesophenocrysts		in ocelli	Mesophenocrysts			Cpx Microphenocrysts					Cpx in glomerophyres
	Rim	Inter	Core	Rim	Inter	Core		Rim	Core		Rim	Inter	Core	Rim	Inter	Core	Rim	Core	
SiO_2	46.36	49.45	47.12	51.47	46.90	52.21	51.40	47.44	46.38	52.05	47.98	44.97	48.17	43.65	50.03	49.42	40.55	46.37	47.62
TiO_2	2.76	1.41	2.16	0.70	2.68	0.34	0.85	2.81	3.01	1.44	2.78	3.49	2.73	4.79	1.86	1.75	5.51	3.20	2.42
Al_2O_3	6.06	5.25	8.45	4.61	5.39	4.32	5.69	5.56	5.85	2.06	4.63	6.97	4.59	7.99	3.36	3.45	9.92	5.88	5.03
$FeO_{(t)}$	7.36	5.07	6.02	5.36	6.67	5.47	5.17	6.55	7.15	6.41	6.79	7.14	6.81	7.52	5.56	5.91	8.46	6.50	6.77
MnO	0.08	0.09	0.10	0.09	0.13	0.15	0.07	0.14	0.10	0.15	0.08	0.10	0.10	0.13	0.11	0.07	0.09	0.09	0.15
MgO	12.82	14.14	12.67	16.44	12.75	17.02	15.87	13.37	13.06	14.03	13.42	12.08	13.76	11.58	14.41	14.36	10.51	12.98	13.39
CaO	23.65	23.25	22.71	19.51	23.50	18.42	18.92	24.13	23.61	23.56	23.91	23.35	23.63	23.59	23.59	22.94	22.75	23.10	22.75
Cr_2O_3	0.08	0.79	0.21	0.35	0.00	0.52	0.72	0.00	0.03	0.67	0.01	0.18	0.13	0.01	0.47	0.24	0.02	0.39	0.11
NiO	0.00	0.00	0.00	0.00	0.00	0.00	0.00	0.00	0.00	0.00	0.00	0.00	0.00	0.00	0.00	0.00	0.00	0.00	0.00
Na_2O	0.16	0.74	0.56	0.76	0.30	0.90	0.94	0.26	0.26	0.01	0.72	0.25	0.39	0.54	0.40	0.48	0.80	0.42	0.49
K_2O	0.01	0.01	0.00	0.02	0.00	0.02	0.02	0.01	0.02	0.02	0.01	0.01	0.01	0.01	0.00	0.02	0.01	0.00	0.05
Total	99.73	100.60	100.21	99.50	98.59	99.55	99.70	100.65	99.96	100.55	100.90	98.88	100.72	100.33	100.02	98.95	99.37	99.26	99.16
FeO	3.92	1.82	3.93	4.17	4.15	4.37	5.15	3.13	3.20	5.05	1.87	4.20	3.30	2.98	3.60	3.30	1.73	3.57	3.52
Fe_2O_3	3.82	3.60	2.32	1.32	2.80	1.22	0.02	3.80	4.38	1.51	5.47	3.27	3.90	5.06	2.18	2.90	7.47	3.26	3.61
Structural formula based on 6 oxygens																			
Si	1.74	1.81	1.74	1.89	1.77	1.91	1.88	1.76	1.73	1.92	1.77	1.70	1.78	1.64	1.85	1.85	1.54	1.74	1.79
Al IV	0.26	0.19	0.26	0.11	0.23	0.09	0.12	0.24	0.26	0.08	0.20	0.30	0.20	0.35	0.15	0.15	0.44	0.26	0.21
Fe^{3+}	0.00	0.00	0.00	0.00	0.00	0.00	0.00	0.00	0.01	0.00	0.03	0.00	0.02	0.01	0.00	0.00	0.01	0.00	0.00
Site T	2.00	2.00	2.00	2.00	2.00	2.00	2.00	2.00	2.00	2.00	2.00	2.00	2.00	2.00	2.00	2.00	2.00	2.00	2.00
Al VI	0.01	0.04	0.11	0.08	0.01	0.09	0.12	0.00	0.00	0.01	0.00	0.02	0.00	0.00	0.00	0.00	0.00	0.00	0.01
Ti	0.08	0.04	0.06	0.02	0.08	0.01	0.02	0.08	0.08	0.04	0.08	0.10	0.08	0.14	0.05	0.05	0.16	0.09	0.07
Fe^{3+}	0.11	0.10	0.07	0.03	0.08	0.03	0.00	0.11	0.11	0.04	0.12	0.09	0.09	0.13	0.06	0.08	0.20	0.09	0.10
Fe^{2+}	0.12	0.06	0.12	0.13	0.13	0.13	0.16	0.10	0.10	0.16	0.06	0.13	0.10	0.09	0.11	0.10	0.05	0.11	0.11
Mn	0.00	0.00	0.00	0.00	0.00	0.00	0.00	0.00	0.00	0.00	0.00	0.00	0.00	0.00	0.00	0.00	0.00	0.00	0.00
Mg	0.72	0.77	0.70	0.90	0.72	0.93	0.86	0.74	0.73	0.77	0.74	0.68	0.76	0.65	0.80	0.80	0.60	0.73	0.75
Cr	0.00	0.02	0.01	0.01	0.00	0.02	0.02	0.00	0.00	0.00	0.00	0.01	0.00	0.00	0.01	0.01	0.00	0.01	0.00
Site M1	1.04	1.03	1.06	1.18	1.03	1.21	1.19	1.02	1.03	1.02	1.00	1.03	1.03	1.01	1.04	1.05	1.01	1.04	1.05
Ca	0.95	0.91	0.90	0.77	0.95	0.72	0.74	0.96	0.95	0.93	0.95	0.95	0.94	0.95	0.94	0.92	0.93	0.93	0.91
Na	0.01	0.05	0.04	0.05	0.02	0.06	0.07	0.02	0.02	0.05	0.05	0.02	0.03	0.04	0.03	0.03	0.06	0.03	0.04
K	0.00	0.00	0.00	0.00	0.00	0.00	0.00	0.00	0.00	0.00	0.00	0.00	0.00	0.00	0.00	0.00	0.00	0.00	0.00
Site M2	0.96	0.97	0.94	0.82	0.97	0.79	0.81	0.98	0.97	0.98	1.00	0.97	0.97	0.99	0.96	0.95	0.99	0.96	0.95
Wo	50.06	49.59	50.42	41.89	50.59	39.72	42.00	50.00	50.44	49.00	49.93	51.06	49.12	51.76	49.16	48.25	51.73	49.95	48.75
En	37.77	41.98	39.14	49.13	38.20	51.07	49.05	39.25	38.37	40.60	39.00	36.76	39.82	35.36	41.79	42.04	33.25	39.07	39.93
Fs	12.17	8.43	10.43	8.98	11.20	9.21	8.96	10.75	11.19	10.41	11.07	12.18	11.06	12.89	9.05	9.71	15.01	10.97	11.33
Mg#*	75.63	83.27	78.96	84.54	77.32	84.72	84.56	78.44	76.51	79.59	77.90	75.11	78.27	73.29	82.20	81.24	68.90	78.07	77.90

*Mg# =100*Mg/(Mg+Fetot)

Table 5 Representative electron microprobe analyses of clinopyroxene minerals of the Río Grande subvolcanic rocks

	Sample P8														
	Green Phenocrysts						Colourless crysts				Inclusion in cognate lithics	in Xenoliths**			Poikilitic phenocryst with apatite inclusion
	Phenocrysts				Microphenocrysts		5		6						
	1		2		3	4									
	Rim	Core	Rim	Core			Rim	Core	Rim	Core	7	8	9	10	11
SiO_2	48.00	51.91	46.44	51.34	53.27	51.41	48.26	52.10	46.85	50.81	53.11	53.64	53.50	53.03	52.18
TiO_2	1.52	0.54	3.06	0.80	0.25	0.42	1.60	0.87	2.34	1.09	0.37	0.15	0.48	0.19	0.23
Al_2O_3	5.50	3.27	6.84	3.21	1.36	4.54	4.80	3.96	6.73	5.68	1.30	4.00	4.23	0.95	1.88
$FeO_{(t)}$	7.67	9.53	6.37	10.24	7.63	7.89	7.79	6.80	7.82	6.73	7.35	3.31	4.38	7.37	8.89
MnO	0.14	0.19	0.06	0.22	0.21	0.16	0.16	0.15	0.20	0.12	0.31	0.06	0.14	0.19	0.23
MgO	12.46	11.21	13.13	11.12	13.43	12.65	12.73	14.15	11.95	13.53	13.78	16.07	15.50	14.01	14.08
CaO	22.81	20.06	23.92	20.30	20.90	21.60	22.64	20.94	22.66	20.71	21.06	19.33	19.20	20.95	19.47
Cr_2O_3	0.02	0.00	0.00	0.03	0.20	0.00	0.01	0.55	0.05	0.30	0.07	1.11	0.84	0.15	0.01
NiO	0.00	0.08	0.03	0.00	0.00	0.03	0.00	0.00	0.05	0.00	0.05	0.06	0.03	0.01	0.02
Na_2O	0.82	2.51	0.44	2.35	2.06	1.15	0.53	1.24	0.89	1.37	1.65	1.71	2.09	1.50	1.72
K_2O	0.00	0.00	0.01	0.02	0.02	0.00	0.00	0.00	0.02	0.02	0.02	0.01	0.02	0.02	0.01
Total	99.41	99.80	100.77	100.19	99.81	100.02	98.83	100.95	100.07	100.58	99.40	99.52	100.64	98.68	99.21
FeO	3.40	5.08	2.14	5.11	3.38	6.10	4.85	5.13	3.34	4.59	4.25	2.86	2.25	4.57	4.32
Fe_2O_3	4.75	4.97	4.70	5.70	4.73	1.95	3.27	1.85	4.98	2.38	3.45	0.50	2.37	3.11	5.08
Structural formula based on 6 oxygens															
Si	1.80	1.93	1.72	1.91	1.97	1.90	1.82	1.90	1.75	1.86	1.97	1.95	1.93	1.98	1.94
Al IV	0.20	0.07	0.28	0.09	0.03	0.10	0.18	0.10	0.25	0.14	0.03	0.05	0.07	0.02	0.06
Fe^{3+}	0.00	0.00	0.00	0.00	0.00	0.00	0.00	0.00	0.00	0.00	0.00	0.00	0.00	0.00	0.00
Site T	2.00	2.00	2.00	2.00	2.00	2.00	2.00	2.00	2.00	2.00	2.00	2.00	2.00	2.00	2.00
Al VI	0.04	0.08	0.01	0.05	0.03	0.10	0.03	0.07	0.05	0.10	0.03	0.12	0.11	0.02	0.03
Ti	0.04	0.02	0.09	0.02	0.01	0.01	0.05	0.02	0.07	0.03	0.01	0.00	0.01	0.01	0.01
Fe^{3+}	0.13	0.14	0.13	0.16	0.13	0.05	0.09	0.05	0.14	0.07	0.10	0.01	0.06	0.09	0.14
Fe^{2+}	0.11	0.16	0.07	0.16	0.10	0.19	0.15	0.16	0.11	0.14	0.13	0.09	0.07	0.14	0.13
Mn	0.00	0.01	0.00	0.01	0.01	0.00	0.01	0.00	0.01	0.00	0.01	0.00	0.00	0.01	0.01
Mg	0.70	0.62	0.72	0.62	0.74	0.70	0.72	0.77	0.67	0.74	0.76	0.87	0.83	0.78	0.78
Cr	0.00	0.00	0.00	0.00	0.01	0.00	0.00	0.02	0.00	0.01	0.00	0.03	0.02	0.00	0.00
Site M1	1.03	1.02	1.02	1.02	1.02	1.06	1.05	1.09	1.03	1.09	1.04	1.13	1.11	1.05	1.10
Ca	0.92	0.80	0.95	0.81	0.83	0.86	0.92	0.82	0.91	0.81	0.84	0.75	0.74	0.84	0.78
Na	0.06	0.18	0.03	0.17	0.15	0.08	0.04	0.09	0.06	0.10	0.12	0.12	0.15	0.11	0.12
K	0.00	0.00	0.00	0.00	0.00	0.00	0.00	0.00	0.00	0.00	0.00	0.00	0.00	0.00	0.00
Site M2	0.97	0.98	0.98	0.98	0.98	0.94	0.95	0.91	0.97	0.91	0.96	0.87	0.89	0.95	0.90
Wo	49.44	46.54	50.72	46.38	45.89	47.65	48.76	45.58	49.92	46.23	45.81	43.66	43.45	45.35	42.32
En	37.59	36.19	38.74	35.37	41.04	38.82	38.15	42.86	36.63	42.04	41.70	50.50	48.82	42.20	42.60
Fs	12.97	17.27	10.55	18.26	13.08	13.53	13.09	11.56	13.45	11.72	12.49	5.84	7.74	12.45	15.08
Mg#*	74.35	67.70	78.60	65.95	75.83	74.15	74.45	78.76	73.14	78.20	76.96	89.64	86.32	77.22	73.86

*Mg# =100*Mg/(Mg+Fetot)

**Xenoliths: 8 and 9, from cpx-bearing carbonate xenoliths and 10, amphibole-cpx xenolith.

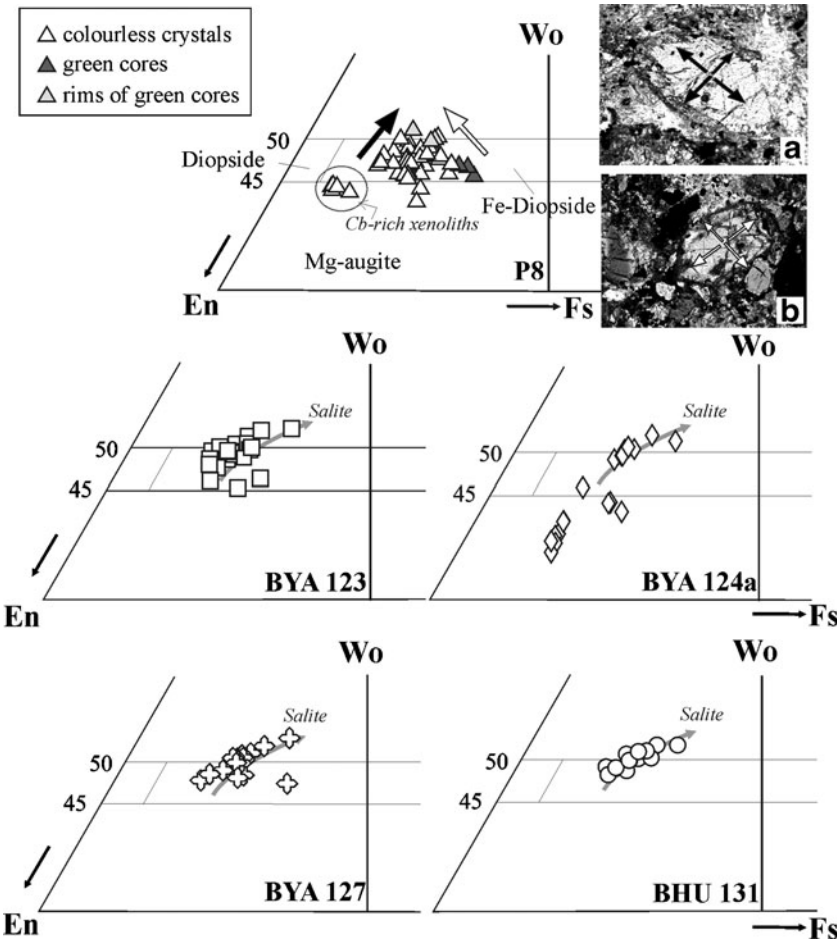

Fig. 6 Representative clinopyroxene compositions for five selected samples from Río Grande subvolcanic rocks. Wollastonite (Wo)-Enstatite (En)-Ferrosilite (Fs) classification diagram (after Morimoto et al. 1988). Microphotographs of the two types of clinopyroxenes of sample P8 are shown: **a** colourless clinopyroxenes and **b** green-core clinopyroxenes

two different varieties of phenocrysts (*brown core amphiboles and green core amphiboles*) and on crystals from cognate lithics. Representative analyses are presented in Table 6. The amphiboles belong to the calcic group (Fig. 8a) with $(Ca+Na)_B>1.00$ and $Na_B<0.50$ (Leake et al. 1997). All crystals have pargasitic compositions ($Al^{IV}>Fe^{+3}$) and due to their Ti apfu content ($0.25<Ti<0.49$) they classify as titanian pargasite. The cognate lithics are richer in Si with two crystals plotting in the edenitic field (Si in formula > 6.5).

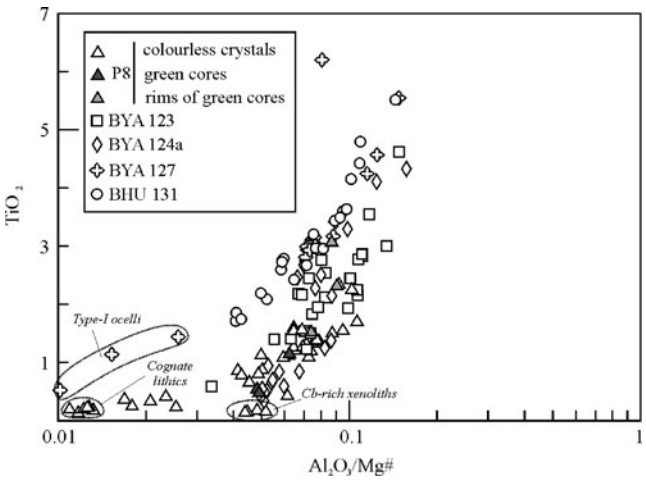

Fig. 7 Al_2O_3/Mg# vs. TiO_2 diagram showing two compositional trends for clinopyroxenes on the basis of increasing TiO_2 contents

The green-core amphibole group shows important compositional zoning characterized by an increase in TiO_2 and decrease in Na_2O (Fig. 8b) from cores to rims. They have high Na_2O (3.98–4.30 wt. %), low TiO_2 (1.24 to 1.70 wt. %), high Al_2O_3 (13.0 wt. %) and Mg# varying between 0.65 and 0.71. The brown-core amphibole group exhibits minor compositional zoning with high TiO_2 (4 wt. %), Mg# between 0.63–0.70 and low Al_2O_3 (12.5 wt. %). The rims of the two types have approximately the same composition with TiO_2 (~3.5 wt. %), low Na_2O (2.5–3.13 wt. %) and Mg# between 0.65 and 0.71.

Mica

The representative compositions of mica listed in Table 7 include phenocryst, microphenocryst/mesophenocryst analyses. Micas from cognate lithics (sample P8) and globular structures (sample BHU 131) have also been analyzed. In the diagram Si apfu vs. $Mg/Mg+Fe^{+2}$ (Fig. 9;

Table 6 Representative electron microprobe analyses of amphibole minerals of the Río Grande subvolcanic rocks

	Sample P8										
	Brown-core Amphibole				Green-core Amphibole					Cognate lithics	
	1		2		3		4			5	6
	Rim	Inter	Rim	Core	Rim	Core	Rim	Inter	Core		
SiO_2	41.22	40.75	40.30	40.99	40.13	41.01	41.49	41.30	42.77	43.53	44.24
TiO_2	2.84	3.99	3.90	4.15	3.96	1.24	3.46	1.22	1.40	2.97	2.33
Al_2O_3	12.07	12.62	13.16	12.45	12.97	14.45	11.28	14.12	13.38	11.57	10.11
Fe_2O_3	1.33	0.47	0.06	0.82	0.56	3.07	0.31	3.12	2.52	0.19	2.04
FeO	8.84	11.74	10.38	12.61	10.09	10.70	13.37	8.92	9.46	8.47	10.45
Cr_2O_3	0.00	0.07	0.03	0.00	0.01	0.00	0.07	0.01	0.00	0.47	0.21
MnO	0.17	0.13	0.14	0.17	0.14	0.25	0.24	0.23	0.30	0.10	0.20
MgO	14.57	12.19	13.41	11.67	13.69	11.13	11.48	12.54	12.80	15.27	13.79
CaO	11.90	10.64	11.99	10.58	11.94	9.63	11.24	10.14	9.76	11.39	10.10
Na_2O	2.74	2.80	2.29	2.70	2.50	4.02	3.13	3.74	3.98	3.29	4.20
K_2O	1.42	2.11	1.99	2.00	1.90	1.06	1.86	1.29	1.33	1.25	1.15
Total	97.08	97.50	97.65	98.15	97.89	96.55	97.94	96.60	97.69	98.51	98.82
Structural formula based on 23 oxygens											
Si	6.11	6.09	5.98	6.10	5.95	6.14	6.22	6.15	6.28	6.30	6.46
AlIV	1.89	1.91	2.02	1.90	2.05	1.86	1.78	1.85	1.72	1.70	1.54
Site T	8.00	8.00	8.00	8.00	8.00	8.00	8.00	8.00	8.00	8.00	8.00
AlVI	0.22	0.31	0.28	0.29	0.21	0.69	0.22	0.62	0.60	0.28	0.20
Fe^{3+}	0.15	0.05	0.01	0.09	0.06	0.35	0.04	0.35	0.28	0.02	0.22
Ti	0.32	0.45	0.44	0.46	0.44	0.14	0.39	0.14	0.15	0.32	0.26
Cr	0.00	0.01	0.00	0.00	0.00	0.00	0.01	0.00	0.00	0.05	0.02
Mg	3.22	2.72	2.97	2.59	3.03	2.49	2.57	2.78	2.80	3.29	3.00
Fe^{2+}	1.09	1.47	1.29	1.57	1.25	1.33	1.68	1.11	1.16	1.03	1.28
Zn	0.00	0.00	0.00	0.00	0.00	0.00	0.00	0.00	0.00	0.00	0.00
Mn	0.00	0.00	0.02	0.00	0.01	0.00	0.03	0.00	0.00	0.01	0.02
Site C	5.00	5.00	5.00	5.00	5.00	5.00	4.93	5.00	5.00	5.00	5.00
Mg	0.00	0.00	0.00	0.00	0.00	0.00	0.00	0.00	0.00	0.00	0.00
Fe^{2+}	0.00	0.00	0.00	0.00	0.00	0.01	0.00	0.00	0.00	0.00	0.00
Zn	0.00	0.00	0.00	0.00	0.00	0.00	0.00	0.00	0.00	0.00	0.00
Mn	0.02	0.01	0.00	0.02	0.01	0.03	0.00	0.03	0.04	0.01	0.01
Ca	1.89	1.70	1.91	1.69	1.90	1.54	1.81	1.62	1.54	1.77	1.58
Na	0.09	0.28	0.09	0.29	0.09	0.42	0.19	0.36	0.43	0.23	0.41
Site B	2.00	2.00	2.00	2.00	2.00	2.00	2.00	2.00	2.00	2.00	2.00
Na	0.70	0.53	0.57	0.49	0.63	0.75	0.72	0.72	0.71	0.70	0.78
K	0.27	0.40	0.38	0.38	0.36	0.20	0.36	0.24	0.25	0.23	0.21
Site A	0.97	0.93	0.95	0.87	0.99	0.95	1.07	0.97	0.96	0.93	0.99
(Ca+Na)B	1.98	1.99	2.00	1.97	1.99	1.96	2.00	1.97	1.96	1.99	1.99
NaB	0.09	0.28	0.09	0.29	0.09	0.42	0.19	0.36	0.43	0.23	0.41
CaB	1.89	1.70	1.91	1.69	1.90	1.54	1.81	1.62	1.54	1.77	1.58
(Na+K)A	0.97	0.93	0.95	0.87	0.99	0.95	1.07	0.97	0.96	0.93	0.99
Si	6.11	6.09	5.98	6.10	5.95	6.14	6.22	6.15	6.28	6.30	6.46
Mg/(Mg+Fe2+)	0.75	0.65	0.70	0.62	0.71	0.65	0.60	0.71	0.71	0.76	0.70

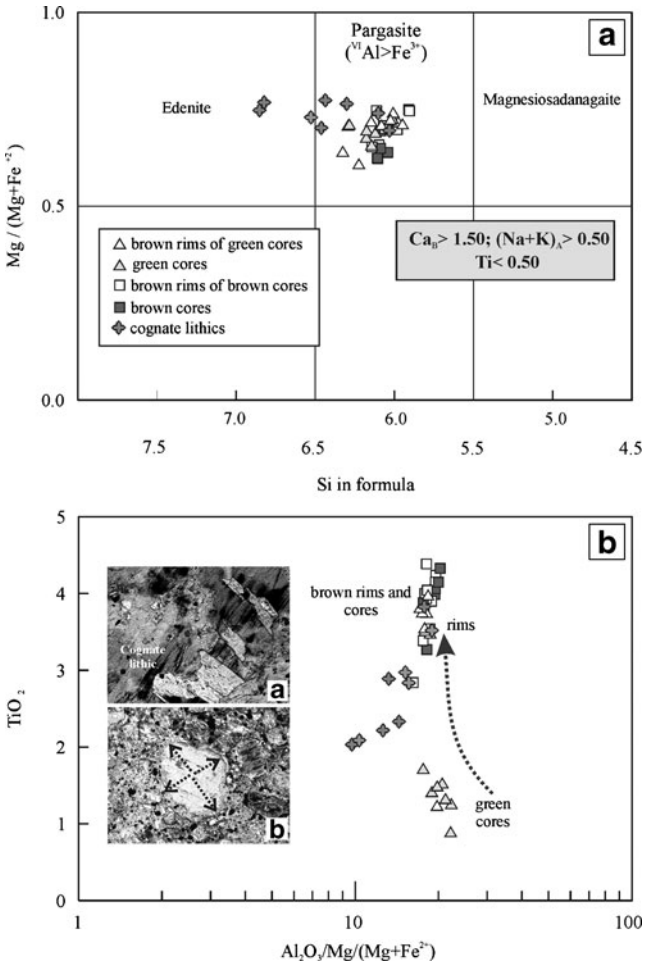

Fig. 8 **a** Classification diagram for amphiboles from sample P8 (after Leake et al. 1997). All crystals are plotted in the calcic amphiboles field and are classified as Titanian-Pargasite. **b** Al_2O_3/Mg# vs. TiO_2 diagram showing the compositional variation for green-core and brown-core amphiboles and xenoliths crystals. Arrows show the core to rim evolution. Microphotographs of A) Cognate lithic and B) Green-core amphibole are shown

Rieder et al. 1998) two groups of mica can be defined. One group, which plots close to the biotite-phlogopite boundary with Mg/Mg+Fe^{+2} ratios between 0.61 and 0.66, is represented by cores of phenocrysts in sample P8, microcrysts of samples BYA 124 and BYA 127 and microphenocrysts inside and around the globular structures of sample BHU 131. A second group, with Mg/Mg+Fe^{+2} ratios between 0.67 and 0.96, is represented by rims of phenocrysts, microphenocrysts and mica in cognate lithics of sample P8. Mica from sample BYA 127 shows a wide variation of Mg# probably due to different degrees of oxidation. A phlogopite included in an olivine phenocryst core, in sample BYA 127 show the highest Mg# of 0.96.

In sample P8 the phenocrysts are characterized by a decrease in TiO_2 and Al_2O_3 contents and increase in Mg/Mg+Fe^{+2} and BaO contents from cores to rims. Biotites related to ocelli and segregations are characterized by lower Mg and higher TiO_2 (from 5.59 to 7.88 wt. %), Al_2O_3 (from 14.5 to 16.0 wt. %) and BaO (from 0.43 to 2.08 wt. %) contents.

Apatite

Apatite was only found in sample P8. The apatite compositions in Table 8 represent one phenocryst apatite and apatite inclusions in a poikilitic macrocryst of clinopyroxene. The phenocryst has higher SrO contents (1.08 wt. %), compared to the apatite inclusions (0.30 to 0.43 wt. % SrO).

Analcime

Analcime is a subordinate phase in the groundmass, but an important mineral in ocelli and segregations. Its composition is homogeneous with 57 wt. % SiO_2, 24 wt. % Al_2O_3 and 13 wt. % Na_2O and very low CaO and K_2O contents (Table 9).

Carbonate

Carbonates have been analyzed (Table 10) in groundmass, clinopyroxene-bearing carbonatite-like xenoliths and globular structures (ocelli and segregations). Most of the analyzed carbonates are dolomite in composition. Breunnerite compositions only occur in segregations. The carbonate from the carbonatite-like xenolith is rich in Sr (2.5–3.0 wt. % $SrCO_3$) and moderately rich in Ba (0.2 wt. % $BaCO_3$).

Analytical procedures

Samples for geochemical analyses were washed and weathered and veined surfaces were cut off. The rocks were crushed and milled in a vídea mill to a very fine powder. Major elements and Ni and Sc (ppm) were analyzed by ICP-OES and trace element analyses were carried out by ICP-MS at ACME Laboratories in Canada.

Sm-Nd and Rb-Sr isotopic analyses followed the method described by Gioia and Pimentel (2000) and were carried out at the Geochronology Laboratory of the University of Brasilia, Brazil. Whole-rock powders (~100 mg) were mixed with ^{149}Sm-^{150}Nd spike solution and dissolved in savillex capsules. Sr, Sm and Nd extraction of whole rock samples followed conventional cation exchange techniques, with Teflon columns containing LN-Spec resin (HDEHP-diethylhexil phosphoric acid supported on PTFE powder). Sr, Sm and Nd samples were loaded on Re evaporation filaments of double filament assemblies, and the isotopic measurements were carried out on a multicollector

Table 7 Representative electron microprobe analyses of mica minerals of the Río Grande subvolcanic rocks

	P8									BHU 131			BYA 123	BYA 127		
	Phenocrysts				Meso- and Microphenocrysts			Inclusion (edenite)	Amphibole rim	in Bt-rich segregations			in Cb-rich segregations	in Cb-rich segregations	in Ocelli	Ol core
	1		2		3	4	5	6	7	8		9	10	11	12	13
	Rim	Core	Rim	Inter						Rim	Core					
SiO_2	37.61	36.57	35.80	36.17	37.47	39.27	38.24	38.89	37.41	35.49	34.25	34.25	34.67	33.61	36.96	39.48
TiO_2	3.24	5.23	6.06	6.29	3.19	2.68	2.87	3.13	3.16	6.82	7.88	7.85	5.76	5.59	3.68	0.50
Al_2O_3	14.99	14.83	15.24	15.27	14.30	14.76	14.06	14.16	14.86	14.79	15.51	15.33	15.52	14.51	10.11	11.79
FeO	7.06	13.21	13.62	13.82	7.42	6.61	7.29	11.90	7.16	11.43	10.23	11.90	12.94	12.39	22.30	13.33
Fe_2O_3	0.00	0.00	0.00	0.00	0.00	0.00	0.00	0.00	0.00	1.06	2.08	1.49	0.48	2.19	4.83	0.00
Cr_2O_3	0.00	0.00	0.00	0.00	0.00	0.00	0.00	0.00	0.00	0.00	0.00	0.00	0.00	0.00	0.00	0.00
MnO	0.22	0.04	0.10	0.11	0.15	0.19	0.17	0.12	0.16	0.10	0.10	0.06	0.11	0.25	0.43	0.33
MgO	20.67	15.29	14.62	14.30	20.80	21.21	21.12	18.85	20.97	14.96	14.86	13.38	15.63	14.14	9.37	20.21
CaO	0.04	0.03	0.00	0.01	0.04	0.11	0.08	0.01	0.07	0.11	0.05	0.12	0.08	0.29	0.21	0.04
Na_2O	0.40	0.82	0.60	0.72	0.68	0.89	0.61	1.36	0.74	0.38	0.46	0.75	0.35	0.27	0.00	0.81
K_2O	9.12	9.23	9.16	9.19	9.26	9.04	9.37	8.31	8.92	8.64	8.71	8.47	9.22	9.10	9.49	8.56
BaO	1.14	0.28	0.00	0.00	1.03	0.74	1.17	0.00	1.57	0.98	2.00	1.39	0.43	2.08	0.00	0.20
Cl	0.00	0.03	0.02	0.02	0.01	0.00	0.00	0.02	0.00	0.02	0.00	0.02	0.02	0.01	0.02	0.01
H2O	4.09	4.02	4.01	4.03	4.06	4.16	4.09	4.14	4.01	3.99	4.02	3.96	3.99	3.88	3.86	4.05
Total	98.57	99.58	99.24	99.92	98.38	99.67	99.07	100.90	99.03	98.75	100.14	98.95	99.18	98.29	101.25	99.30
Structural formula based on 22 oxygens																
Si	5.51	5.44	5.34	5.36	5.52	5.65	5.59	5.62	5.48	5.33	5.13	5.19	5.21	5.22	5.80	5.84
Al^{IV}	2.49	2.56	2.66	2.64	2.48	2.35	2.41	2.38	2.52	2.62	2.74	2.74	2.75	2.65	1.87	2.05
Fe^{3+}	0.00	0.00	0.00	0.00	0.00	0.00	0.00	0.00	0.00	0.05	0.14	0.08	0.05	0.13	0.33	0.11
Site T	8.00	8.00	8.00	8.00	8.00	8.00	8.00	8.00	8.00	8.00	8.00	8.00	8.00	8.00	8.00	8.00
Al^{VI}	0.10	0.04	0.03	0.03	0.00	0.15	0.01	0.03	0.04	0.00	0.00	0.00	0.00	0.00	0.00	0.00
Fe_t^{2+}	0.86	1.64	1.70	1.71	0.91	0.79	0.89	1.44	0.88	1.38	1.14	1.43	1.58	1.48	2.59	1.45
Fe^{3+}	0.00	0.00	0.00	0.00	0.00	0.00	0.00	0.00	0.00	0.07	0.10	0.09	0.01	0.12	0.24	0.00
Ti	0.36	0.59	0.68	0.70	0.35	0.29	0.32	0.34	0.35	0.77	0.89	0.89	0.65	0.65	0.43	0.06
Mg	4.51	3.39	3.25	3.16	4.57	4.55	4.60	4.06	4.57	3.35	3.32	3.02	3.50	3.27	2.19	4.45
Mn	0.03	0.01	0.01	0.01	0.02	0.02	0.02	0.01	0.02	0.01	0.01	0.01	0.01	0.03	0.06	0.04
Site O	5.86	5.66	5.67	5.62	5.85	5.80	5.84	5.88	5.86	5.58	5.46	5.44	5.75	5.56	5.51	6.00
Ca	0.01	0.00	0.00	0.00	0.01	0.02	0.01	0.00	0.01	0.02	0.01	0.02	0.01	0.05	0.04	0.01
Na	0.11	0.24	0.17	0.21	0.19	0.25	0.17	0.38	0.21	0.11	0.13	0.22	0.10	0.08	0.00	0.23
K	0.85	0.88	0.87	0.87	0.87	0.83	0.87	0.77	0.83	1.66	1.66	1.64	1.77	1.80	1.90	1.61
Ba	0.13	0.03	0.00	0.00	0.12	0.08	0.13	0.00	0.18	0.06	0.12	0.08	0.03	0.13	0.00	0.01
Site A	1.10	1.15	1.05	1.08	1.19	1.18	1.19	1.15	1.23	1.78	1.80	1.88	1.88	1.93	1.93	1.85
Cations	14.96	14.81	14.72	14.70	15.04	14.98	15.04	15.03	15.09	15.36	15.26	15.32	15.63	15.49	15.45	15.85
$Mg/(Mg+Fe^{+2})$	0.84	0.67	0.66	0.65	0.83	0.85	0.84	0.74	0.84	0.69	0.71	0.66	0.68	0.66	0.41	0.96
$Fe^{+2}/(Fe^{+2}+Mg)$	0.16	0.33	0.34	0.35	0.17	0.15	0.16	0.26	0.16	0.31	0.29	0.34	0.32	0.34	0.59	0.03

Obs: H_2O recalculated by stoichiometry. Fe_2O_3 only recalculated for samples with deficiency in tetrahedral site.

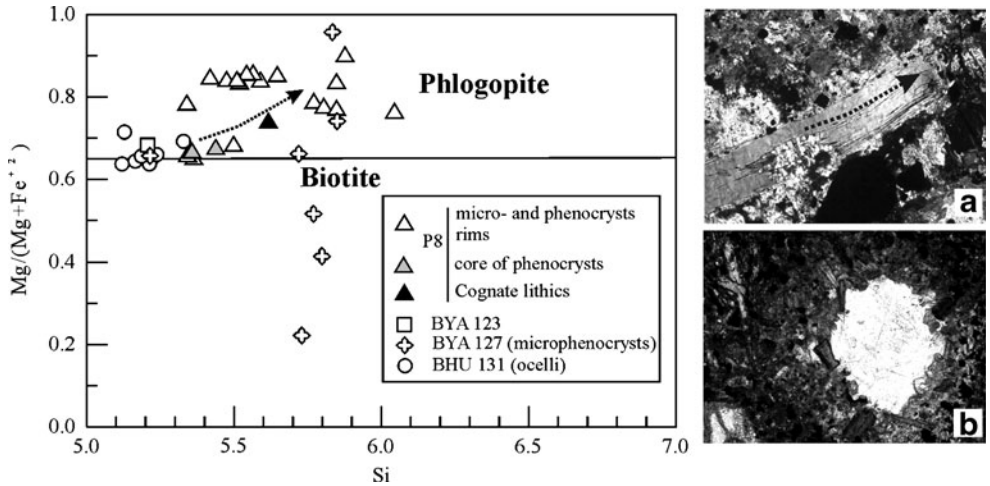

Fig. 9 Classification diagram for mica compositions (after Rieder et al. 1998)

Table 8 Representative electron microprobe analyses of apatite minerals of the Río Grande subvolcanic rocks

	Sample P8		
	Phenocryst	Inclusions in Cpx phenocrysts	
	1	2	3
SiO_2	0.00	0.13	0.12
Al_2O_3	0.00	0.00	0.01
MgO	0.14	0.38	0.34
Fe_2O_3	0.34	0.34	0.32
CaO	53.31	53.83	54.50
Na_2O	0.35	0.06	0.12
K_2O	0.00	0.01	0.03
P_2O_5	41.67	40.14	40.51
Cl	0.24	0.13	0.11
SrO	1.08	0.43	0.31
BaO	0.01	0.00	0.00
H_2O_3	1.70	1.69	1.72
Total	98.83	97.14	98.07
Cations per formula unit			
Na	0.12	0.02	0.04
Si	0.00	0.02	0.02
Al	0.00	0.00	0.00
Mg	0.04	0.10	0.09
K	0.00	0.00	0.01
P	6.02	5.90	5.90
Ca	9.74	10.02	10.04
Cl	−0.05	−0.03	−0.02
Sr	0.11	0.04	0.03
Fe	0.05	0.05	0.05
Ba	0.00	0.00	0.00
H	0.56	0.57	0.57
Cations	16.57	16.69	16.71

Finnigan MAT 262 mass spectrometer in static mode. Uncertainties on $^{87}Sr/^{86}Sr$ ratios were better than ±0.01% (2σ) and of Sm/Nd and $^{143}Nd/^{144}Nd$ ratios were better than ±0.2% (2σ) and ±0.005% (2σ), respectively, according to repeated analyses of international rock standards BHVO-1 and BCR-1. $^{143}Nd/^{144}Nd$ ratios were normalized to $^{146}Nd/^{144}Nd$ of 0.7219, and the decay constant used was 6.54×10^{-12} y^{-1}. The T_{DM} values were calculated using DePaolo's model (1981).

The K-Ar age was obtained at the CPGeo (Center for Geochronological Research) of the University of São Paulo. Gases were extracted from samples and purified using a high-vacuum extraction line. 40Ar* concentration was determined using an "off-line" gas source Reynolds-type mass spectrometer and K concentration was obtained using a conventional flame photometry technique, in a Micronal B462 photometer. A detailed description of this methodology is reported in Amaral et al. (1966).

Geochemical characteristics

Alteration

Most of the selected rocks are fresh to moderately altered (Table 1) and characterized by a groundmass with variable amounts of carbonate and analcime. In all bulk chemical analyses, loss on ignition (LOI) values are high, varying from 5.9 to 22.8%., as a common feature of lamprophyre rocks (Rock 1991; Nedli and Tóth 2007). High water content in Río Grande lamprophyres are attested by the abundance of Titanian pargasite and biotite/phlogopite phenocrysts in the *amphibole-bearing olivine-free group*, and the abundance of biotite/phlogopite microphenocrysts in the *olivine-bearing amphibole-free group.* Such high water contents characterized not only the magma source but

Table 9 Representative electron microprobe analyses of analcime minerals of the Río Grande subvolcanic rocks

	BYA 123		BHU 131		P8						
	in Ocelli		in Ocelli	in Bt-rich segregation	in Ocelli				in Groundmass		
	1	2	3	4	5	6	7	8	9	10	11
SiO_2	54.66	59.20	61.92	58.02	57.23	53.20	55.76	52.18	62.77	50.61	52.08
Al_2O_3	25.46	24.85	22.71	24.91	24.63	23.73	21.17	24.92	22.47	22.72	23.19
FeO	0.51	0.13	0.18	0.16	0.01	0.07	0.09	0.63	0.26	0.04	1.23
CaO	0.69	0.05	0.01	0.13	0.00	0.30	0.11	0.63	0.08	0.29	0.32
Na_2O	10.46	13.58	12.18	12.24	13.26	12.93	13.96	10.92	10.91	11.46	11.85
K_2O	0.20	0.08	0.08	0.05	0.04	0.25	0.12	0.34	0.09	0.27	0.55
Total	91.99	97.90	97.08	95.50	95.28	90.49	91.30	89.62	96.69	85.42	89.23
Cations calculated on the basis of 7 oxygens											
Si	2.29	2.48	2.59	2.43	2.39	2.23	2.33	2.18	2.63	2.12	2.18
Al	1.26	1.22	1.12	1.23	1.21	1.17	1.04	1.23	1.11	1.12	1.14
Sum T	3.54	3.70	3.71	3.65	3.61	3.39	3.38	3.41	3.73	3.24	3.32
Fe_t^{2+}	0.02	0.00	0.01	0.01	0.00	0.00	0.00	0.02	0.01	0.00	0.04
Ca	0.03	0.00	0.00	0.01	0.00	0.01	0.01	0.03	0.00	0.01	0.01
Na	0.85	1.10	0.99	0.99	1.08	1.05	1.13	0.89	0.88	0.93	0.96
K	0.01	0.00	0.00	0.00	0.00	0.01	0.01	0.02	0.00	0.01	0.03
Sum A	0.91	1.11	1.00	1.01	1.08	1.08	1.15	0.95	0.90	0.96	1.05
Cations	4.45	4.81	4.71	4.66	4.69	4.47	4.52	4.37	4.64	4.20	4.37

also the late stage of evolution when groundmass analcime and carbonate crystallized. At this stage, the H_2O content could have been enough to allow separation of a fluid phase from the melt.

The high volatile contents observed in the fresh and altered samples from Río Grande lamprophyres may also be interpreted in part as CO_2 derived from primary or secondary carbonate. The mineral chemistry analyses revealed that the dolomite of some xenoliths and ocelli show high SrO and BaO contents (Table 10) that is common in magmatic carbonate. On the other hand the host sedimentary rocks do not have hydrothermal or metamorphic alteration that could explain the presence of secondary carbonate. Taking into account this evidence we considered that the carbonate of the studied lamprophyre rocks might be the result of late magmatic autometasomatic processes such as circulation of H_2O- and CO_2-rich volatiles, occurring extensively in lamprophyres (Rock 1991; Vichi et al. 2005).

Whole-rock chemistry

Major and trace element analyses were carried out on eleven selected samples (Table 11). The analyzed samples show high TiO_2 (up to 4.83%) and MgO (~ 10%) but variable concentrations of Na_2O (0.09–3.65) and K_2O (0.87–1.9 wt. %). For classification purposes we used the Nb/Y vs. Zr/TiO_2 diagram (Winchester and Floyd 1977) normally used in the literature for lamprophyre classification (e.g. Nedli and Tóth 2007). The diagram (Fig. 10) shows that the Río Grande lamprophyres have transitional compositions between alkali basalts and basanites/nephelinites, similar to the composition of alkaline lamprophyre monchiquites (Rock 1991).

High contents of compatible trace elements (164–253 ppm Cr, 152–423 ppm Ni, 17–24 ppm Sc, 44–95 ppm Co and 202–400 ppm V) indicate small degrees of fractionation (Table 11). The wide range in some incompatible trace elements (229–1666 ppm Ba, 356–2590 ppm Sr, 22–75 ppm Rb and 57–251 ppm Nb) may reflect alteration, although similarly high concentrations and wide variations of LILE have been described for several lamprophyres (e.g. Rock 1991; Azambre et al. 1992; Szabó et al. 1993; Dostal and Owen 1998; Ngounouno et al. 2005; Nedli and Tóth 2007). Sample P8 displays the highest contents of Ba, Sr, Nb and LREE.

The trace element compositions normalized to chondrites (Thompson 1982) show enrichment in LILE and LREE with values from 50 to approximately 800 times the chondritic values (Fig. 11a). The HREE and HFSE contents range from 6 to approximately 200 times the chondritic values. Evident negative K and Sr anomalies together with a small negative Ti anomaly are observed. A monchiquite (Rock 1991) and ocean island basalt (Sun and McDonough 1989) are shown for comparison.

Table 10 Representative electron microprobe analyses of carbonate minerals of the Río Grande subvolcanic rocks

	Sample P8										BHU 131				BYA 123	BYA 124
	in Type-II ocelli			in Groundmass					Carbonate xenoliths		in Type-I ocelli			in segregations	in Type-III ocelli	in Type-III ocelli
	1	2	3	4	5	6	7	8	9	10	11	12	13	14	15	16
FeO	15.77	17.70	15.87	13.02	16.01	14.05	12.85	14.68	11.77	9.21	12.70	9.69	7.08	45.15	8.62	12.12
MnO	0.91	0.96	1.16	1.09	1.36	1.10	0.73	1.82	0.22	0.37	0.56	0.68	0.75	0.13	1.12	0.57
MgO	30.07	28.63	30.19	28.35	26.32	30.73	33.19	28.74	29.77	35.41	30.73	34.43	33.91	51.40	30.92	33.86
CaO	50.81	50.39	51.67	54.75	52.64	51.35	51.11	51.77	53.32	51.89	51.20	52.15	55.63	2.07	57.30	52.19
SrO	0.45	0.47	0.62	0.96	0.71	0.48	0.39	1.13	3.09	2.50	2.06	0.80	0.45	0.02	0.04	0.15
BaO	0.00	0.00	0.00	0.00	0.00	0.00	0.00	0.05	0.22	0.07	0.00	0.00	0.18	0.05	0.00	0.00
C	1.34	1.33	1.36	1.34	1.31	1.34	1.35	1.33	1.34	1.37	1.33	1.35	1.36	1.35	1.35	1.37
Total	99.35	99.47	100.88	99.50	98.35	99.05	99.61	99.52	99.72	100.80	98.57	99.10	99.34	100.16	99.35	100.25
Cations per formula unit																
Ca	1.00	1.00	1.01	1.05	1.05	0.52	1.00	1.03	1.05	1.00	1.02	1.02	1.08	0.04	1.07	0.95
Mg	0.71	0.67	0.70	0.65	0.63	0.37	0.77	0.68	0.70	0.81	0.73	0.80	0.78	1.09	0.68	0.73
Fe	0.27	0.30	0.27	0.22	0.28	0.12	0.22	0.25	0.20	0.15	0.22	0.16	0.12	0.70	0.14	0.19
Ba	0.00	0.00	0.00	0.00	0.00	0.00	0.00	0.00	0.00	0.00	0.00	0.00	0.00	0.00	0.00	0.00
Sr	0.01	0.01	0.01	0.01	0.01	0.00	0.01	0.02	0.04	0.03	0.03	0.01	0.01	0.00	0.00	0.00
Mn	0.02	0.02	0.02	0.02	0.02	0.01	0.01	0.03	0.00	0.01	0.01	0.01	0.01	0.00	0.02	0.01
C	0.00	0.01	0.00	0.06	0.01	0.97	0.00	0.00	0.00	0.00	0.00	0.00	0.00	0.17	0.10	0.12
Cations	2.00	2.00	2.00	2.00	2.00	2.00	2.00	2.00	2.00	2.00	2.00	2.00	2.00	2.00	2.00	2.00

Table 11 Representative major and trace elements analyses from the Río Grande subvolcanic rocks

Groups	Amphibole free, olivine bearing group									Amphibole bearing, olivine free group	
Locality sample	Coraya			Yacoraite					Huichaira	Yacoraite	
	BCO 49	BCO 51	BCO 52	BYA 122	BYA 123	BYA 124a	BYA 125	BYA 127	BHU 131	P8	BYA 126
Major oxides (wt%)											
SiO_2	33.55	52.71	33.50	38.54	38.05	38.03	28.53	35.24	37.45	26.48	28.80
TiO_2	2.72	3.54	4.83	2.56	2.71	2.73	3.68	3.35	3.93	2.52	4.22
Al_2O_3	8.72	9.43	14.05	14.20	9.71	9.24	10.63	9.27	10.32	7.11	9.72
$Fe_2O_{3\ (t)}$	14.12	14.81	25.81	11.73	13.15	11.40	8.22	13.44	12.85	12.09	17.94
MnO	0.20	0.29	0.08	0.20	0.17	0.15	0.43	0.21	0.16	0.34	0.35
MgO	12.67	1.77	6.91	7.26	12.19	9.97	8.48	11.43	9.96	10.99	9.46
CaO	9.48	6.06	3.26	7.05	11.60	9.43	14.18	13.15	10.96	16.76	10.01
Na_2O	0.17	0.06	2.32	3.65	1.50	1.42	0.09	2.12	2.90	2.89	0.11
K_2O	0.54	1.90	0.71	1.63	1.78	1.56	1.21	1.71	0.87	0.89	1.07
P_2O_5	1.14	0.98	2.28	1.33	1.04	0.58	1.42	1.32	0.97	1.99	1.68
L.O.I	16.40	8.20	5.90	11.50	7.60	15.20	22.80	8.30	9.30	17.50	16.30
Total	99.71	99.75	99.65	99.65	99.50	99.71	99.67	99.54	99.67	99.56	99.66
Trace elements (ppm)											
Be	3	4	4	4	2	3	2	3	3	4	4
Sc	24	17	24	19	20	23	22	19	18	16	19
Ti	16306	21222	28956	15347	16246	16366	22062	20083	23560	15120	25299
V	202	242	400	234	219	218	218	256	263	190	269
Cr	250	226	253	75	164	226	178	171	164	109	113
Co	84	47	69	44	63	68	73	69	59	73	95
Ni	423	244	350	95	177	324	257	193	152	141	240
Cu	31	165	47	108	85	89	86	71	77	56	66
Zn	157	70	156	122	73	89	127	105	56	104	400
Ga	14	10	25	26	17	16	20	19	21	14	27
As	8	28	14	9	6	10	12	4	17	12	4
Se	b.d.l	1	1	1	1	b.d.l	1	b.d.l	1	b.d.l	b.d.l
Rb	22	75	26	63	62	52	57	71	35	27	56
Sr	356	275	413	754	1041	712	828	1657	812	2589	437
Y	29	31	56	45	29	21	47	38	31	67	56
Zr	223	283	416	303	254	180	404	311	316	259	507
Nb	80	89	171	115	100	58	129	138	91	251	193
Mo	1	1	1	3	4	2	0	0	2	16	1
Ag	b.d.l	b.d.l	b.d.l	0	b.d.l	0	0	b.d.l	b.d.l	b.d.l	b.d.l
Cd	0	0	b.d.l	0	0	0	0	0	0	0	0
Sn	1	2	3	3	2	1	2	2	2	2	2
Sb	1	2	2	0	0	0	0	b.d.l	0	0	0
Cs	4	6	7	5	12	8	41	36	87	39	27
Ba	318	315	283	394	1008	466	229	1016	881	1666	324
Hf	6	7	9	7	6	5	9	7	7	5	12
Ta	4	6	9	6	6	4	8	8	6	8	13
W	16	35	20	39	40	38	47	58	49	55	10
Au*	7	17	11	14	b.d.l	31	14	51	b.d.l	9	10
Hg	b.d.l	b.d.l	b.d.l	b.d.l	0	0	0	b.d.l	0	0	0
Tl	0	0	0	0	0	0	0	0	0	0	0
Pb	33	74	38	11	7	65	26	5	3	22	20

Table 11 (continued)

Groups	Amphibole free, olivine bearing group									Amphibole bearing, olivine free group	
Locality sample	Coraya			Yacoraite					Huichaira	Yacoraite	
	BCO 49	BCO 51	BCO 52	BYA 122	BYA 123	BYA 124a	BYA 125	BYA 127	BHU 131	P8	BYA 126
Bi	b.d.l	1	0	0	b.d.l	b.d.l	0	b.d.l	b.d.l	0	b.d.l
Th	10	10	27	21	13	7	17	15	11	57	19
U	3	13	7	5	3	2	6	4	2	11	7
Rare earth elements (ppm)											
La	88	83	182	117	97	56	134	132	81	298	139
Ce	180	175	371	244	198	112	288	262	170	570	284
Pr	18	17	35	24	19	11	28	25	18	57	27
Nd	66	66	134	89	70	44	106	93	68	190	103
Sm	12	12	23	15	12	8	18	16	12	28	18
Eu	4	4	7	4	3	2	6	5	4	7	6
Gd	9	10	19	12	9	6	15	12	10	19	15
Tb	1	1	3	2	1	1	2	2	1	3	2
Dy	6	7	13	9	6	4	9	8	7	13	11
Ho	1	1	2	2	1	1	2	1	1	2	2
Er	3	3	5	4	3	2	4	3	3	5	5
Tm	0	0	1	1	0	0	1	0	0	1	1
Yb	2	2	4	3	2	1	3	3	2	4	4
Lu	0	0	0	1	0	0	0	0	0	1	0
La/Yb_n	29	25	32	23	37	28	33	35	27	53	25
La/Sm_n	5	4	5	5	5	4	5	5	4	11	5
Gd/Yb_n	4	4	4	3	4	4	4	4	4	5	3

(*) concentrations of Au element in ppb

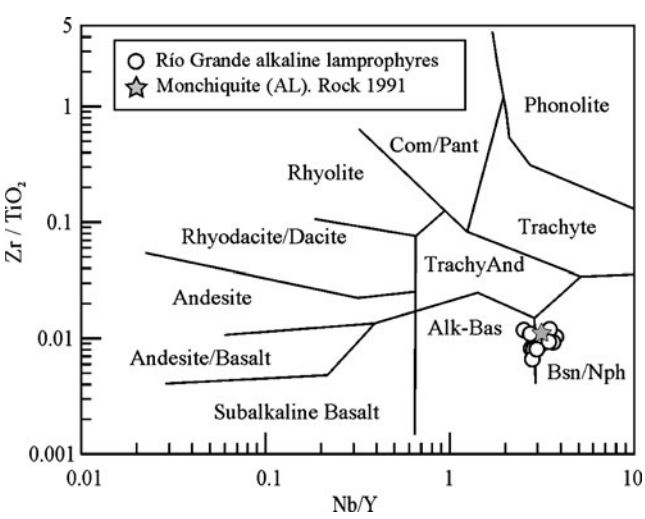

Fig. 10 Rock classification diagram using Zr, Ti, Nb and Y immobile elements (Winchester and Floyd 1977) for the Río Grande subvolcanic rocks

Total REE concentrations range from 376 to 798 ppm (Table 11). Chondrite-normalized trace element patterns (Sun and McDonough 1989) are characterized by strong LREE enrichment and REE fractionation with $(La/Yb)_n$ ratio varying from 23.1 to 36.8 for all samples except for sample P8. The $(La/Sm)_n$ and $(Gd/Yb)_n$ values from 4.15 to 5.06 and from 2.79 to 4.36 respectively, indicate that garnet was not an important phase in the source (Fig. 11b). Sample P8 has a higher $(La/Yb)_n$ ratio of 53.08, with $(La/Sm)_n$ and $(Gd/Yb)_n$ values, 10.65 and 5.01 respectively, indicating a stronger enrichment in LREE with respect to the other samples. This enrichment may be due to the presence in the groundmass of magmatic carbonatitic material (see Fig. 5). The lack of a Eu anomaly suggests that plagioclase fractionation (either by crystal fractionation or upper crustal contamination) was not important during the origin and differentiation of the original magma.

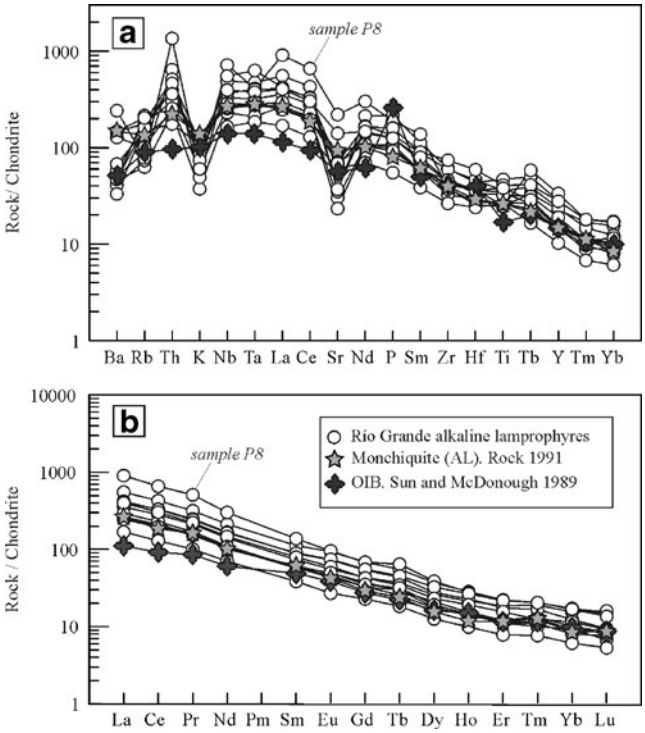

Fig. 11 **a** Chondrite normalized abundance spidergrams (Thompson 1982) and **b** REE normalized diagram (Sun and McDonough 1989) for the Río Grande rocks. For comparison monchiquite-alkaline lamprophyres (Rock 1991) and average ocean island basalt (OIB; Sun and McDonough 1989) are shown

Geochronology and isotopic data

K-Ar data

Biotite macrocrysts and microcrysts (up to 2 cm) were separated from two samples (BYA 126 and P8) for K-Ar geochronology. The analyses (Table 12) resulted in K-Ar ages of 190±11 Ma (sample BYA 126) and 163±9 Ma (sample P8). These two K-Ar ages even considering the analytical uncertainties, are not overlapping. The discrepancy between the two ages may be due the alteration of sample BYA 126. For this reason we consider the 163± *9 Ma* age of sample P8 as the representative age of this group of lamprophyres.

Sr and Nd isotopic data

Nine samples for whole rock Nd isotopic analyses and six samples for whole rock Sr isotope analyses were selected. Sm and Nd concentration were determined by isotopic dilution, whereas ICP-MS was used for determination of Rb and Sr contents (Table 13). Initial Sr and Nd isotopic ratios have been re-calculated at *163 Ma* (Fig. 15).

The Río Grande rocks display a notable variation in initial $^{87}Sr/^{86}Sr$ isotopic ratios. Samples BCO 49, BYA 124a, BYA 125 and BHU 131 have moderately high initial $^{87}Sr/^{86}Sr$ isotopic ratios ranging from 0.70724 to 0.70781, whereas samples P8 and BYA 127, present lower Sr initial ratios of 0.70377 and 0.70455, respectively. The εNd (t) values are positive, ranging between + 1.5 (sample BHU 131) and + 5.6 (sample BYA 124a). T_{DM} model ages vary between 250 and 640 Ma (Table 13).

Discussion

Lamprophyres are melanocratic hypabyssal igneous rocks rich in H_2O and/or CO_2 (e.g. Rock 1991) characterized by porphyritic textures and mafic phenocrysts. Their petrogenesis is complex and they are considered to represent mantle-derived magmas, some of which were generated at considerable depths (100–150 km) (e.g. Rock 1991; Bernard-Griffiths et al. 1991; Bédard 1994; Nedli and Tóth 2007).

Three main types of lamprophyres are described in the literature: calc-alkaline lamprophyres (CAL), alkaline lamprophyres (AL) and ultramafic lamprophyres (UML) (Rock 1987, 1991). They are all considerably enriched in volatile elements (H_2O, CO_2, F, Cl), and in LILE. The group of calc-alkaline lamprophyres consists mainly of the rock-types minette, vogesite, kersantite, spessartite, appinite and kentallenite, which correspond roughly to basaltic-andesite composition but are considerably enriched in some elements (K, Rb, Ba, Mg, Cr, Ni, etc) and more closely approximated geochemically by some shoshonites and absarokites (Rock 1987, 1991). The group of alkaline lamprophyres consists mainly of the rock-types camptonite, monchiquite and sannaite (Rock 1991) which correspond

Table 12 K-Ar biotite age data for the Río Grande subvolcanic rocks

Sample	Rock type	Mineral	Age (Ma)	Max. Error (2 sigma)	Ar^{40} rad ccSTP/g (*10^{-6})	Ar^{40} atm (%)	% K	K error (%)
BYA 126	alkaline-lamprophyre	bt	190.3	10.6	44.60	15.01	5.7341	3.9326
P8	alkaline-lamprophyre	bt	163.1	8.3	33.05	17.16	4.9917	3.1034

Table 13 Rb-Sr and Sm-Nd isotopic data for the Río Grande subvolcanic rocks

Locality	Sample	Rb (**) ppm	Sr (**) ppm	$^{87}Rb/^{86}Sr$	$(^{87}Sr/^{86}Sr)_{meas}$	$(^{87}Sr/^{86}Sr)$ T	Sm (ppm)	Nd (ppm)	$^{147}Sm/^{144}Nd$	$(^{143}Nd/^{144}Nd)_{meas}$	$(^{143}Nd/^{144}Nd)$ T	$\varepsilon_{Nd\ (0)}$	$\varepsilon_{Nd\ (T)}$	T_{DM} (Ga)
Coraya	BCO 49	22.00	356.00	0.01	0.70756 (±02)	0.70715	13.38	66.10	0.12	0.512752 (±06)	0.512621	2.21	3.77	0.51
	BCO 52						25.38	136.21	0.11	0.512753 (±06)	0.512633	2.25	4.00	0.46
Yacoraite	P8	27.00	2589.00	*0.105	*0.70373 (±02)	0.70377	25.07	159.24	0.10	0.512635 (±05)	0.512533	−0.05	2.06	0.54
	BYA 123						12.73	74.40	0.10	0.512752 (±06)	0.512642	2.23	4.17	0.42
	BYA 124a	52.10	712.30	0.361	0.70829 (±02)	0.70781	7.94	41.21	0.12	0.512716 (±11)	0.512716	1.53	5.62	0.25
	BYA 125	57.10	828.40	0.541	0.70783 (±01)	0.70737	18.24	100.84	0.11	0.512747 (±16)	0.512630	2.13	3.95	0.45
	BYA 126						18.23	100.73	0.11	0.512743 (±15)	0.512626	2.05	3.87	0.46
	BYA 127	71.20	1657.40	0.308	0.70484 (±01)	0.70455	15.78	90.19	0.11	0.512735 (±07)	0.512622	1.89	3.79	0.46
Huichaira	BHU 131	35.20	812.40	0.13	0.70753 (±03)	0.70724	13.21	71.68	0.11	0.512625 (±06)	0.512506	−0.03	1.52	0.64

Obs:
Uncertainties on measured isotope ratios are given in parenthesis (2s)
ε_{Nd} (T) calculated relative to CHUR with present-day value of $^{143}Nd/^{144}Nd$=0.512638. T_{DM} values were calculated using De Paolo' model (1981).
$^{87}Sr/^{86}Sr$ and $^{143}Nd/^{144}Nd$ and $\varepsilon_{Nd(t)}$ calculate with an age of 163 Ma.
(*) Data from Omarini et al. (2005).
(**) Elemental abundances of Rb and Sr are taken from ICP-MS analyses

broadly to alkali basalts, basanites and nephelinites. Finally the group of ultramafic lamprophyres is formed mainly by rock-types such as aillikite, alnöite, damtjernite, ouachitite and polzenite (Rock 1991), which correspond broadly to melililites and melilite-nephelinites. These different types can occur together in the same region and fortuitous juxtapositions of lamprophyres of different ages and compositions are common (Rock 1987, 1991).

Three processes can be involved in the origin of lamprophyres: 1) partial melting of metasomatic sub-continental lithospheric mantle in subduction-related or rift-related tectonic settings; 2) contamination of mantle-derived mafic magmas with continental crust; and 3) mixing of basaltic magmas with varying amounts of ultrapotassic lithospheric mantle derived melts during heating and/or thinning processes of sub-continental lithospheric mantle (Rock 1979, 1991; Xu et al. 2007 and references therein).

Petrography and mineral chemistry

Based on their mineral composition, these lamprophyres are classified as monchiquites, a feldspar-free alkaline lamprophyre composed of diopside, Ti-rich biotite/phlogopite, Ti-pargasite, and forsteritic olivine phenocrysts in a groundmass made of the same minerals except olivine, with analcime, carbonate and abundant globular structures (ocelli and segregations). Since analcime is an important phase in the ocelli, the rocks are identified here as *ocellar analcime monchiquites*.

According to the petrographic and mineral chemistry data two groups of monchiquites are recognized in the Río Grande Valley: an *amphibole-bearing olivine-free group*, represented by samples P8 and BYA 126 and an *olivine-bearing amphibole-free group* represented by samples BYA 122, 123, 124a-b, 127 and BHU 131.

The amphibole-bearing olivine-free group

This group is characterized by the presence of phlogopite, apatite, primary analcime and abundant carbonate phase in the groundmass. The P8 sample exhibits two clinopyroxene types: the clinopyroxenes with green cores showing increase in Mg# and decrease in Na_2O contents from core to rims, and the colourless phenocrysts clinopyroxenes showing increase in TiO_2 and decrease in Mg# from core to rims. In the normal evolution of diopside the substitution scheme is the replacement of Ca by Na in the M_2 site, followed by Mg by Fe total substitution. This scheme is followed by colourless phenocrysts suggesting that fractional crystallization operated together with equilibration at low pressure and temperature (Wass 1979). On the contrary, the green cores clinopyroxenes do not follow this scheme,

being considered here as xenocrysts from a more alkaline magma (Rock 1991) suggesting that mixing processes operated during the evolution of magma that formed the Río Grande lamprophyres. The colourless rims of the green cores represent the re-equilibration of these xenocrysts to the new magma conditions. In the diagram MgO/FeO_t vs. SiO_2/TiO_2 (Fig. 12a) clinopyroxenes of sample P8 fall in the AL, CAL and along the AL-UML boundary fields. Clinopyroxenes from cognate lithic and carbonatite-like xenoliths from this sample plotted in the CAL field and near the CAL-LL boundary respectively. The colourless clinopyroxenes fall in the AL field and along the AL-UML field boundary. The green-core clinopyroxenes are plotted in the AL field, whereas their rims fall near the AL-UML boundary, indicating an evolution trend that may be explained by a mixing between an alkaline magma (represented by green cores) and magma with an ultramafic signature, represented by the colourless clinopyroxenes.

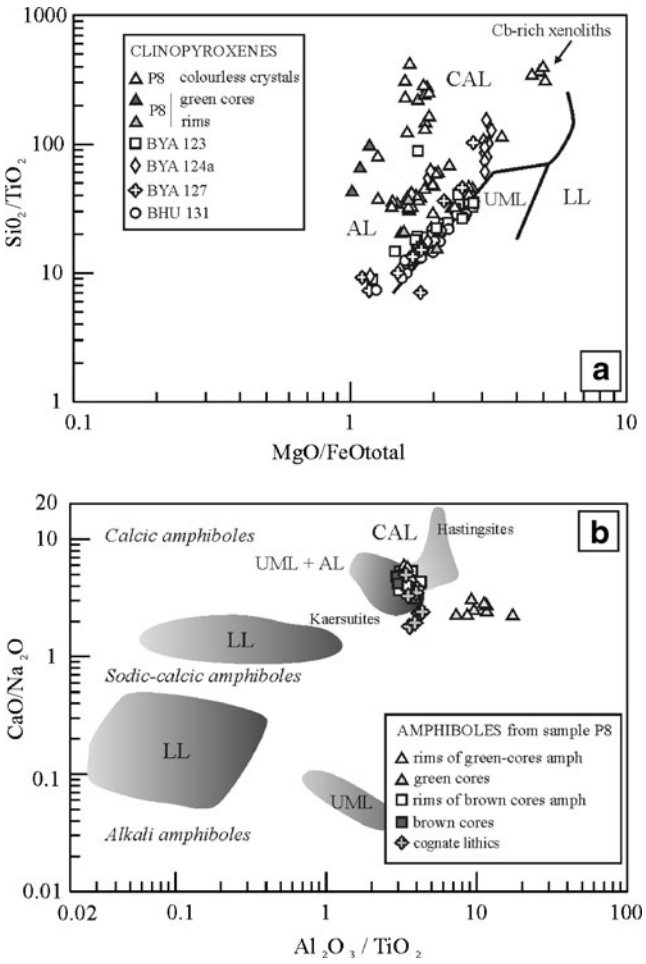

Fig. 12 **a** MgO/FeO_t vs. SiO_2/TiO_2 discrimination diagram for pyroxenes composition in lamprophyres (Rock 1987). **b** Al_2O_3/TiO_2 vs. CaO/Na_2O discrimination diagram for amphibole compositions in lamprophyres (Rock 1987). Symbols: CAL: calc-alkaline lamprophyres, AL: alkaline lamprophyres, UML: ultramafic lamprophyres and LL: lamproites. See text for discussion

Amphibole also exhibits complex compositional variations. The core to rim increase in TiO_2 with no systematic Mg# variation in green-core amphiboles and the decrease in TiO_2 with an increase in Mg# in brown core amphiboles are incompatible with a fractional crystallization processes. The similar composition of the rims of both groups suggests that amphiboles were re-equilibrated at similar conditions. In the Al_2O_3/TiO_2 vs. CaO/Na_2O diagram for amphibole crystals (Fig. 12b) the green-core and brown-core amphiboles show different behavior. The green-core amphiboles show the strongest compositional variation from cores to rims: the cores fall outside the fields for the typical lamprophyres and the rims plot between the UML-AL and CAL fields. The brown-core amphiboles show minor variation with cores plotting in the UML-AL field near the CAL boundary and the rims falling in the CAL fields. The presence of two different types of amphiboles may be explained by mixing processes. The rims of two amphibole types having similar composition suggest that they crystallized under equilibrated conditions in hybrid magma. The crystals from the cognate lithics have variable compositions with some grains plotted along the UML-AL/CAL boundary.

The phlogopite crystals are characterized by an increase in Mg# and Ba and decrease in TiO_2 and Al_2O_3 contents from core to rims indicating that mixing processes occurred during magma differentiation. The rims of phlogopite phenocrysts have the same composition as the groundmass phlogopite suggesting that they were comfortable with the new conditions of the hybrid magma.

The complex and contrasting compositional variations shown by the main mineral phases suggest that mixing represents the most important process during the differentiation of magma. Our mineral chemistry data suggest that a volatile-rich high TiO_2 alkaline magma (AL) mixed, before emplacement, with a low TiO_2-high Mg# ultramafic liquid (UML).

The presence of carbonatite-like xenoliths and the abundant Sr-and Ba-rich carbonate in the groundmass could indicate the suggestive intervention of a carbonatitic liquid with CAL signature during magma evolution.

The olivine-bearing amphibole-free group

This group is characterized by a groundmass with abundant ocelli and an analcime/carbonate ratio higher than that of the amphibole-bearing group. The biotite/phlogopite is restricted to the groundmass and often associated with ocelli and segregation structures. The clinopyroxenes show an increase in TiO_2 content and a decrease in Mg# from core to rims. In the diagram MgO/FeO_t vs. SiO_2/TiO_2 (Fig. 12a), the clinopyroxenes of sample BYA 123 are plotted along the AL-UML boundary field, except one core that falls in the CAL field. In the sample BYA 124a the

clinopyroxene cores generally plotted in the CAL field whereas the rims fall along the AL-UML boundary, suggesting a change in the magma conditions from calc-alkaline to alkaline conditions during their crystallization. The clinopyroxene compositions of sample BHU 131 fall along the AL-UML boundary with increasing TiO_2 contents from cores to rims. The biotite/phlogopite is characterized by high TiO_2 content and relatively low Mg#, similar in composition to the cores of phlogopite crystals in sample P8. In sample BYA 127 a phlogopite, included in the core of an olivine phenocryst, shows the highest Mg# (~96) and the lowest TiO_2 content, suggesting that it crystallized in magma with a UML signature.

The mineral phases of this group show a normal evolution trend with increase in Ti contents and decrease in Mg#. This behavior is compatible with both fractional crystallization and mixing process between magmas with UML and AL signature. Our data suggest the presence of a volatile-rich, low TiO_2, high Mg# (UML) magma during the very early stage of differentiation, followed by mixing with a high TiO_2 more alkaline magma (AL) as shown by the salitic trend in clinopyroxenes.

Globular structures

Ocelli and segregations have been described in a variety of rock types including basalt (Upton and Wadsworth 1971), spilite (Smith 1967), picrite (Drever 1960) and tholeiitic dolerite (Nakamura and Coombs 1973), but they are most commonly found in lamprophyres (e.g. Phillips 1968; Ferguson and Currie 1971; Philpotts 1972, 1976; Strong and Harris 1974; Cooper 1979; Foley 1984; Rock 1991). Their origin is debated (Rock 1991). They are believed to represent either: (i) magmatic crystallization involving liquid immiscibility (Philpotts 1976; Eby 1980) that produces structures characterized by distinctive chemistry and different rim compositions between the minerals of globules and groundmass (Foley 1984) or (ii) segregations of late stage liquids or amygdales (Cooper 1979; Azbej et al. 2006) that are characterized by low TiO_2 contents relative to the bulk (Philpotts 1976) and are zoned, with an inner analcime-carbonate zone and an outer ground-mass mineral zone (Foley 1984).

The large number of ocelli in the studied rocks suggests a high volatile content for the original magma. In the three types of ocelli identified, the predominance of carbonate minerals over biotite or amphibole in some samples, suggests that CO_2 dominated over H_2O in the gas phase (Nedli and Tóth 2007). The *type I-ocelli* is the least abundant type and it is characterized by the presence of low Ti clinopyroxenes (Fig. 7), which are compositionally different from the other clinopyroxene of the groundmass. According to Foley (1984) they may represent a carbonatite-like melt. The *types II and III ocelli* lack early differentiates, such as olivine and clinopyroxene, and may be explained by late stage segregation processes.

Tectonic and petrogenetic implications

The oldest rocks known to date in the pre-rift phase of the Salta Rift, are the ~150 Ma old (Cristiani 2004; Cristiani et al. 2008; Haschke et al 2005) anorogenic plutonic complexes (Tusaquillas Plutonic Complex, Abra-Laite-Aguilar and Fundiciones complexes) along the Cobres-Salinas Grandes and Tres Cruces branches. Concurring with the K-Ar age of c. 163 Ma of this study, the Río Grande monchiquites preceded the formation of the Salta Rift. They were emplaced along the N-S axis of the main future rift structures and are spatially associated with the magmatism of the pre-rift stage, represented by the Tusaquillas Plutonic Complex OIB-type basic rocks (Fig. 13).

The studied lamprophyres are compared with the igneous rocks from the pre-rift (Tusaquillas Plutonic Complex) and the syn-rift (basanites) stages of the Salta Rift (Fig. 13). The Río Grande lamprophyres are characterized by the highest LILE, HFSE and LREE contents and by pronounced K and Sr negative anomalies. Taking into account that Río Grande lamprophyres are plagioclase-free, the observed Sr negative anomaly could reflect the characteristics of the mantle source. The slightly positive Ta and Nb anomaly in the lamprophyres also suggests that during their petrogenesis a subduction-related component was absent or not important. The geochemical characteristics of lamprophyric magmas could represent the partial melting of

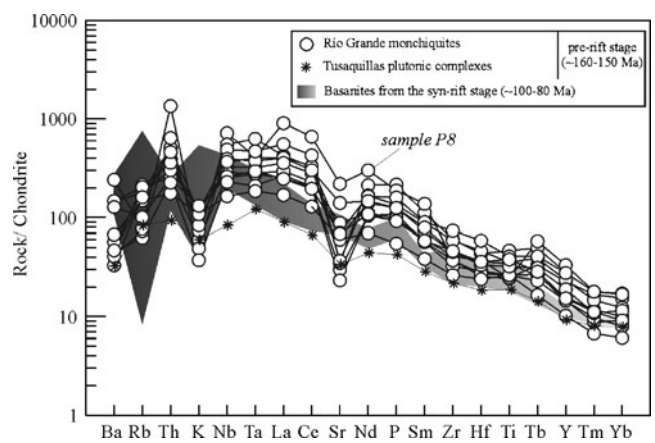

Fig. 13 Comparison of trace elements pattern between the Río Grande lamprophyres and the pre-rift and syn rift ígneous rocks of Salta Rift. The pré-rift stage (~150 Ma) is represented by the Tusaquillas Plutonic Complex (Cristiani 2004) and the syn-rift stage (100 Ma) is represented by the Las Conchas, Finca El Rodeo and Matancillas basanites and El Cadillal phonotephrite rocks (Lucassen et al. 2007). The Río Grande lamprophyres are characterized by the highest LILE and HFSE contents and by a pronounced K and Sr negative anomalies. Normalizing values are from Thompson (1982)

an enriched continental lithospheric mantle, present in this sector of the Central Andes in Mesozoic times, as suggested by several authors (Lucassen et al. 2005, 2007).

The OIB magma of the Tusaquillas Complex, is less enriched in LILE and HFSE, representing the partial melt of the asthenospheric mantle (Cristiani et al. 2005). This suggests that magma alkalinity decreased with time during the development of the pre-rift stage. Alkaline basanitic volcanism that occurred in the syn-rift stage (Fig. 13) is characterized by lower LILE, HFSE and LREE contents compared with Río Grande monchiquites, but it is enriched in these elements when compared to the Tusaquillas Plutonic Complex. The geochemical characteristics of the syn-rift rocks can be explained by the fusion of a depleted lithospheric mantle source (Lucassen et al. 2007).

Therefore the evolution of Salta Rift does not follow the typical magmatic rift evolution (from more alkaline to less alkaline) controlled by progressive lithospheric extension, as occurred in the East African Rift system (Gass 1970) and in the Bohemian Ohre/Eger Rift (Ulrych et al. 2008).

Isotopic composition of the lithospheric mantle

The Río Grande lamprophyres, plotted in the $^{87}Sr/^{86}Sr$ vs εNd (t) diagram (Fig. 14), are compared with other mafic volcanic rocks from the Central Andes and the composition of several types of mantle xenoliths hosted in the Salta Rift basanites. The composition of OIB magma from Tusaquillas Plutonic Complex is also reported. The studied samples fall close to the high-Sr basanite (Lucassen et al. 2005) and within the high $^{87}Sr/^{86}Sr$ peridotite field. On the basis of field, petrographic and geochemical characteristics, we suggest that the variable initial $^{87}Sr/^{86}Sr$ isotopic ratios shown by our samples reflect the primary characteristics of magmas. If we suppose that alteration processes could have modified the isotopic composition leading to higher $^{87}Sr/^{86}Sr$ ratios, it would be difficult to explain the lowest $^{87}Sr/^{86}Sr$ exhibited by the sample P8 characterized by a carbonate-rich groundmass. According to geochemical and isotopic data we suggest that the pristine magmas of the Río Grande lamprophyres originated from an enriched metasomatized lithospheric mantle. The variation in the initial ratios for Nd and Sr also suggests that the mantle source was heterogeneous, with one end-member formed by high $^{87}Sr/^{86}Sr$ ratios and other showing low values for this ratio.

The lithospheric mantle under the Central Andes since the Paleozoic was periodically modified by tectonic and/or subduction processes (Lucassen et al. 2005). Previous research (Lucassen et al. 2007) has identified three chemically and isotopically distinct sub-continental lithospheric mantle (SCLM) reservoirs under the Central Andes: (i) a Proterozoic mantle, belonging to the Brazilian shield, which is thought to be progressively underthrust beneath the present Central Andes during Miocene shortening (e.g., McQuarrie et al. 2005) (ii), an early Paleozoic mantle, which formed, or was modified, during the late Cambrian early Ordovician Famatinian orogeny and (iii) lithospheric mantle modified by magmatic activity during Mesozoic extension (e.g., Viramonte et al. 1999; Sempere et al. 2002).

Several other strands of evidence indicate the presence of metasomatised mantle beneath the Central Andes. Basanitic lavas of the syn-rift stage of the Salta Rift, outcropping 100 km south of the study area, carried mantle xenoliths with metasomatic veins composed of phlogopite, amphibole and apatite (Viramonte et al. 1999). The

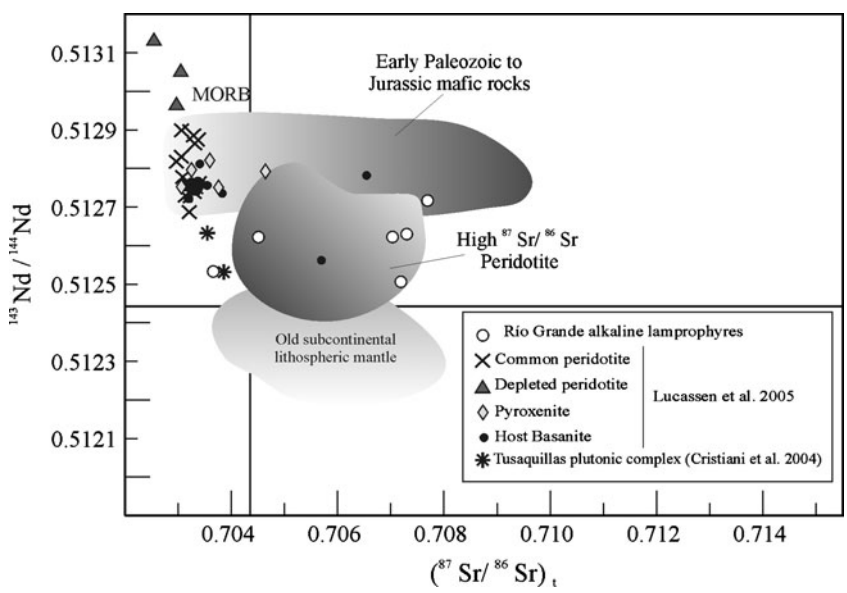

Fig. 14 $^{87}Sr/^{86}Sr$ vs. $^{143}Nd/^{144}Nd$ diagram for the Río Grande lamprophyres. The isotopic compositions of xenoliths and mantle-derived rocks from the Central Andes (Lucassen et al., 2005) are also shown for comparison. The data are recalculated at 160 Ma

Cretaceous (~100 Ma) Ayopaya alkaline province of Central Bolivia (Schultz et al. 2004), associated with the Mesozoic extensional tectonics of South America, also gives information about the composition of the mantle under the Central Andes region. We have compared the Ayopaya alkaline province with the recent alkaline magmatism of Tanzania (Schultz et al. 2004) and suggest the presence of a metasomatised mantle under this sector of South America. Schultz et al. (2004) also reported a kimberlitic dyke with characteristics similar to sample P8.

Petrogenetic model

In order to understand the petrogenesis of the lamprophyres of Río Grande Valley, we modeled partial melting processes that occurred in the lithospheric mantle beneath the Salta Rift in Jurassic time.

Modal batch-melting calculations have been carried out for a metasomatized mantle, shown in Fig. 15. Due to the lack of information about the Central Andes lithospheric mantle composition during Jurassic time, we choose an amphibole lherzolite (BD3848A) from Pello Hill in Tanzania (Dawson and Smith 1988) as a good proxy to the original mantle composition. The mantle xenoliths from the Salta rift (Lucassen et al. 2002, 2005) are hosted in Cretaceous basanites (Fig. 15) and represent the composition of a mantle that probably had already undergone partial melting and metasomatic processes during the early stages of the Salta rift. For this reason we prefer to use for our modeling a mantle composition typical of a region, such as Tanzania, characterized by a pre-rift or early syn-rift stage, comparable with Ayopaya alkaline province region of Bolivia (Schultz et al. 2004).

The modeled lherzolite is characterized by 6.0 ppm of Ce and 0.16 ppm of Yb. For the clinopyroxene and phlogopite we used the partition coefficients for alkaline lamprophyres (Foley et al. 1996), whereas for the remaining minerals we used the partition coefficients for basaltic liquids (Rollinson 1993).

Partial melting trajectories suggest that the Río Grande lamprophyres could be generated by less than 3 % partial melting of an amphibole-bearing lherzolitic mantle source (Fig. 15). The different lamprophyre samples could have been formed by nearly the same degree of melting of the same source. The BYA 123 and BYA 124a compositions may be explained by partial melting of an amphibole lherzolite with Ol (79.6%), Cpx (12.8%), Amp (2.6%) and Phlo (5%), whereas samples BYA 127 and BYA 122 could be explained only by approximately 0.5% partial melting of an amphibole lherzolite with Ol (85%), Cpx (5.7%) and Phlo (9.3%). However this last melting degree is too low for the melt to be extracted efficiently from the mantle. The composition of the remaining samples may be modeled using a source with mineral compositions which are intermediate between those two described above. The presence, in the sublithospheric mantle, of metasomatic veins constituted by apatite, phlogopite and other accessory phases (as suggested by the xenolith reported by Viramonte et al. 1999), would modify notably the behavior of trace elements during partial melting processes. For this reason a realistic alternative is that the studied lamprophyres with different geochemical characteristics may be derived by partial melting of a heterogeneous metasomatic lithospheric mantle.

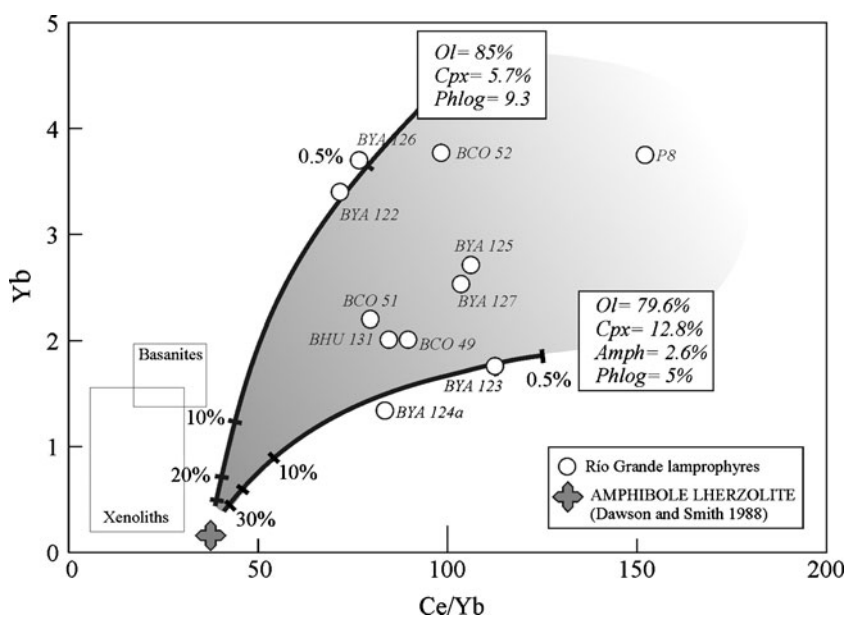

Fig. 15 Ce/Yb vs. Yb diagram showing batch-melting model. An amphibole lherzolite (sample BD3438A, Pello Hill, Tanzania) represents the metasomatised mantle source. Degree of partial melting (%) is indicated along the melting lines

Type of mantle metasomatism

Around the world, several types of metasomatic processes have been identified on the basis of chemical, isotopic, and mineralogical compositions of mantle xenoliths. Proposed metasomatic agents include alkali-rich silicate and $CO_2 \pm H_2O$-rich fluids or carbonatite melts (e.g. Frey and Green 1974; Roden et al. 1984; Coltorti et al. 1999). The REE patterns of the studied rocks show strong enrichment in LREE, with noticeable depletion in the HREE. The assumed introduction of a CO_2-rich fluid in the depleted mantle source might have increased LREE with respect to HREE (Barbieri et al. 1997). The anomalous $SrCO_3$ content of carbonate (e.g. ocelli, cpx-bearing carbonate xenoliths and groundmass in sample P8), may also suggest the involvement of carbonatitic liquids during the evolution of the Río Grande monchiquites. The presence of apatite in some xenoliths and as microphenocrysts in sample P8 may also be suggestive of metasomatism by carbonatite melts or CO_2 -rich fluids. This hypothesis is supported by the occurrence of carbonatitic rocks associated with the Salta rift in NW Argentina and Bolivia such as the Santa Julia Complex (Zappettini 1998) and the Ayopaya carbonatite complex (Schultz et al. 2004; Lucassen et al. 2007).

Conclusions

The new data permitted us to classify the Río Grande dikes and sills, define the geological setting of their formation and their petrogenesis, and, finally, constrain the mantle composition beneath the NW Argentina in Jurassic time.

The new petrographic and mineral chemistry data obtained permitted us to classify these rocks as lamprophyres, specifically ocellar alkaline monchiquites.

The clinopyroxene, amphibole and phlogopite compositions suggests the presence of three different magma components (CAL-, AL-, UML- types) that mixed during the petrogenesis of lamprophyres, reflecting heterogeneous lithospheric mantle sources.

The mineral chemistry, geochemical and isotopic characteristics of the Río Grande lamprophyres indicate that they could represent primary magmas derived by partial melting process from a heterogeneous enriched metasomatised lithospheric mantle. These lamprophyric magmas differentiated by magma mixing and fractionation processes during their ascent. The petrographic and geochemical characteristics of Río Grande lamprophyres (e.g. diopside-rich carbonatitic xenoliths, the abundant macrocrysts of biotite/phlogopite and microphenocrysts of apatite in sample P8, the carbonatitic-rich groundmass that characterize all samples) suggest the intervention of a carbonatitic magma component.

The new K/Ar geochronological data (c. 160 Ma) suggest that they are related to the pre-rift stage of the Salta continental rift of NW Argentina. This age permits us to reject the hypothesis proposed by several authors that these subvolcanic rocks were related to the evolution to the Neoproterozoic to lower Paleozoic basement.

Acknowledgements The authors are CNPq and CONICET researchers and grateful for the research grant that allowed field and laboratory work. We also thank financial support from the PROSUL/CNPq program. Bárbara Lima is acknowledged for technical assistance. Dr. Miguel Basei is thanked for the K-Ar ages. We are very grateful to F. Stoppa, K.M Goodenough and anonymous referees for constructive reviews and to K. Moore for careful editorial comments that led to a significant improvement of the paper. Dr. Affonso Brod is thanked for the assistance during the mineral chemistry analyses. We are also grateful to Dr. Affonso Brod and Sérgio Castro Valente for correcting and improving the manuscript.

References

Amaral G, Cordani UG, Kawashita K, Reynolds JH (1966) Potassium-argon dates of basaltic rocks from Southern Brazil. Geochim Cosmochim Acta 30:159–189

Avila Salinas WA (1986) El magmatismo Cretácico en Bolivia. Symposium IGCP Project 242, La Paz, Proceedings, 52–66

Azambre B, Rossy M, Albarede F (1992) Petrology of the alkaline magmatism from the Cretaceous North-Pyrenean Rift Zone (France and Spain). Eur J Mineral 4:813–834

Azbej T, Szabó C, Bodnár RJ, Dobosi G (2006) Genesis of carbonate aggregates in lamprophyres from the northeastern Transdanubian Central Range, Hungary: magmatic or hydrothermal origin? Mineral Petrol 88:479–497

Bahlburg H (1998) The geochemistry and provenance of Ordovician turbidites in the Argentina Puna. In: Pankhurst RJ, Rapela CW (eds) The Proto-Andean margin of Gondwana. Geol Soc London Spec Publ 142: 127–142

Barbieri M, Ghiara MR, Stanzione M, Villar LM, Pezzutti NE, Segal S (1997) Trace-element and isotope constraints on the origin of ultramafic lamprophyres from Los Alisos (Sierras Subandinas, Northern Argentina). J South Amer Earth Sci 10:39–47

Bédard JH (1994) Mesozoic east North American alkaline magmatism: part 1. Evolution of Monteregian lamprophyres, Québec, Canada. Geochim Cosmochim Acta 58:95–112

Bernard-Griffiths J, Fourcade S, Dupuy C (1991) Isotopic study (Sr, Nd, O and C) of lamprophyres and associated dykes from Tamazert (Morocco): crustal contamination processes and source characteristics. Earth Planet Sci Lett 103:190–199

Castaño A, Rodrigo LA (1978) Sinopsis estratigráfica de Bolívia Parte 1: Paleozóico. Publicaciones Academia Nacional de Ciencias Boliviana: 146 pp.

Chayle W, Coira B (1987) Vulcanitas básicas a ultrabásicas y mesosilíceas de la Formación Puncoviscana en el área del Cerro Alto de Minas-Departamento Tilcara-Jujuy, Argentina. X Congr Geol Argentino, Tucumán, Actas 4:292–295

Cherroni C (1977) El sistema Cretácico en la parte boliviana de la cuenca cretácica andina. Revista Técnica YPFB 6(12):5–46

Coira B, Manca N, Chayle W (1990) Registros volcánicos en la Formación Puncoviscana. In: Aceñolaza FG, Millar H, Toselli AJ (eds), El Ciclo Pampeano en el Noroeste Argentino. Serie de Correlación Geológica N 4. Universidad de Tucumán: 53–60

Coltorti M, Bonadiman C, Hinton RW, Siena F, Upton BGJ (1999) Carbonatite metasomatism of the oceanic upper mantle: evidence

for clinopyroxenes and glasses in ultramafic xenoliths of Grande Comoro, Indian Ocean. J Petrol 40:133–165

Comin-Chiaramonti P, Gomes CB, Velázques VF, Censi P, Antonini P, Comin-Chiaramonti F, Punturo R (2005) Alkaline complexes from southeastern Bolivia. In: Comin-Chiaramonti P, Gomes CB (eds) Mesozoic to Cenozoic Magmatism in the Brazilian Platform. EDUSP/FAPESP, São Paulo

Cooper AF (1979) Petrology of ocellar lamprophyres from western Otago, New Zealand. J Petrol 20:139–164

Cristiani C (2004) Il plutonismo anorogenico Mesozoico nell'Altiplano della Puna (Argentina Nord occidentale, Ande Centrali): implicazioni petrogenetiche e geodinamiche. PhD thesis, Universita de Pisa (in italian)

Cristiani C, Matteini M, Mazzuoli R, Omarini RH, Villa IM (2005) Petrology of late Jurassic-early Cretaceous Tusaquillas and Abra Laite-Aguilar Plutonic Complexes (Central Andes, 23º 05′ S-66º 05′ W): a comparison with rift-related magmatism of NW Argentina and E Bolivia. In: Comin-Chiaramonti P, Gomes CB (eds) Mesozoic to Cenozoic magmatism in the Brazilian platform. EDUSP/FAPESP, São Paulo, pp 213–240

Cristiani C, Omarini RH, Matteini M, Mazzuoli R (2008) SHRIMP U-Pb zircon age of the Abra Laite granite: New evidence of the late Jurassic rift-related plutonism in NW-Argentina. In: Linares E, Cabaleri NG, Do Campo MD, Ducós EI, Panarello HO (eds) VI South American Symposium on Isotope Geology, Proceedings in CD-ROM. Buenos Aires

Dawson JB, Smith JV (1988) Metasomatized and veined upper-mantle xenoliths from Pello Hill, Tanzania: evidence for anomalously-high mantle beneath the Tanzania sector of the East African Rift Valley. Contrib Mineral Petrol 100:510–527

Delor CP, Rock NMS (1991) Alkaline-ultramafic lamprophyre dykes from the Vestfold Hills, Princess Elizabeth Land, E. Antarctic. Antarct Sci 3:419–432

DePaolo DJ (1981) A neodymium and strontium isotopic study of Mesozoic calc-alkaline granitic batholith of the Sierra Nevada and Peninsular Ranges. California. J Geophys Res 86:10470–10488

Dostal J, Owen JV (1998) Cretaceous alkaline lamprophyres from northeastern Czech Republic: geochemistry and petrogenesis. Geol Rundsch 87:67–77

Drever HI (1960) Immiscibility in the picritic intrusión at Igdlorssuit, West Greenland. 21st Int Geol Congr 13:47–58

Eby GN (1980) Minor and trace elements partitioning between immiscible ocelli groundmass pairs from lamprophyres dykes and sills, Monteregian Hills petrographic province, Quebec. Contrib Mineral Petrol 75:269–278

Fareeduddin I, Kirmani R, Basavalingu B (2001) Petrology of ocellar lamprophyres in South Delhi Fold Belt, Danva, Sirohi District, Rajasthan, India. Gondwana Res 3:497–508

Ferguson J, Currie KL (1971) Evidence of liquid immiscibility in alkaline ultrabasic dykes at Callander bay, Ontario. J Petrol 12:561–585

Foley SF (1984) Liquid immiscibility and melt segregations in alkaline lamprophyres from Labrador. Lithos 17:127–137

Foley SF, Jackson SE, Fryer BJ, Greenough JD, Genner GA (1996) Trace element partition coefficients for clinopyroxene and phlogopite in an alkaline lamprophyre from Newfoundland by La-ICP-MS. Geochim Cosmochim Acta 60:229–238

Frey FA, Green DH (1974) The mineralogy, geochemistry and origin of lherzolite inclusions in Victorian basanites. Geochim Cosmochim Acta 38:1023–1059

Galliski MA, Viramonte JG (1988) The Cretaceous paleo-rift in northwestern Argentina: a petrologic approach. J South Amer Earth Sci 1:329–242

Gass IG (1970) The evolution of volcanism in the junction area of the Red Sea, Gulf of Aden and Ethiopian rifts. Phil Trans R Soc London 267:369–381

Gioia SMC, Pimentel MM (2000) The Sm-Nd isotopic method in the Geochronology Laboratory of University of Brasilia. An Ac Bras de Ciências 72:219–245

Gomez Omil R, Boll A, Hernandez R (1989) Cuenca Cretácico-Terciaria del noroeste argentino (Grupo Salta). In: Chebli G, Spalleti L (eds) Cuencas Sedimentarias de la República Argentina. Serie de Correlación Geológica N 4 Universidad Nacional de Tucumán

Haschke M, Deeken A, Insel N, Sabel E, Grave M, Schmitt AK (2005) Growth pattern of the Andean Puna plateau constrained by apatite fission track, apatite (U-Th)/He, K-feldspar $^{40}Ar/^{39}Ar$, and zircon U-Pb geochronology. 6th International Symposium on Andean Geodynamics (ISAG 2005, Barcelona). Extended Abstracts: 360–363

Hauser N, Matteini M, Pimentel MM, Omarini RH (2008) K-Ar age and Sr-Nd isotopic geochemistry of alkaline lamprophyre dykes, from the Río Grande Valley, Eastern Cordillera, NW Argentina: Origin of parental magmas from a metasomatized mantle. VI Symposio Sudamerican de Geología Isotópica, San Carlos de Bariloche, Argentina, Proceedings CD-rom

Jacques JM (2003) A tectonostratigraphic synthesis of the Sub-Andean basins: implications for the geotectonic segmentation of the Andean Belt. J Geol Soc London 160:687–701

Jaillard E, Hérail G, Monfret T, Díaz-Martínez E, Baby P, Lavenu A, Mumont JF (2000) Tectonic evolution of the Andes of Ecuador, Peru, Bolivia and Northernmost Chile. In: Cordani UG, Dilani EJ, Thomaz Filho A, Campos DA (eds) Tectonic evolution of South America 31st International Geological Congress, Río de Janeiro: 481–559

Kumpa M, Sanchez MC (1988) Geology and sedimentology of the Cambrian Grupo Mesón (NW Argentina). In: Bahlbur GH, Breitkreuz C, Giese P (eds) The southern Central Andes: contributions to structure and evolution of an active continental margin. Lect Notes Earth Sci 17: 39–53

Lanfranco JJ (1972) Estudio de las intrusiones en la falda oriental de la Sierra de Aguilar y metamorfitas del área de contacto. PhD thesis, Universidad Nacional de Córdoba, 68 pp

Leake BE, Wooley AR, Arps CES, Birch WD, Gilbert MC, Grice JD, Hawthorne FC, Kato A, Kisch HJ, Krivovichev VG, Linthout K, Laird J, Mandarino JA, Maresch WV, Nickel EH, Rock NMS, Schumacher JC, Smith DC, Stephenson NCN, Ungaretti L, Whittaker EJW, Youzhi G (1997) Nomenclature of amphiboles: report of the Subcommittee on Amphiboles of the International Mineralogical Association, Commission on New Minerals and Mineral Names. Am Mineral 82:1019–1037

Lucassen F, Escayola M, Fran G, Rome RL, Koc K (2002) Isotopic composition of Late Mesozoic basic and ultrabasic rocks from the Andes (23º–32º)—implications for the Andean mantle. Contrib Mineral Petrol 143:336–349

Lucassen F, Franz G, Viramonte JG, Romer RL, Dulski P, Lang A (2005) The late Cretaceous lithospheric mantle beneath the central Andes: evidence from phase equilibrium and composition of mantle xenoliths. Lithos 82:379–406

Lucassen F, Franz G, Romer RL, Schultz F, Dulski P, Wemmer K (2007) Pre-Cenozoic intraplate magmatism along the Central Andes (17º–34ºS): composition of the mantle at an active margin. Lithos 99:312–338

Manca N, Coira B, Barber E, Pérez A (1987) Episodios magmáticos de los ciclos Pampeano y Famatiniano en el Río Yacoraite, Jujuy. X Congr Geol Argentino, Tucumán Actas 4:299–301

McQuarrie N, Horton BK, Zandt G, Beck S, DeCelles PG (2005) Lithospheric evolution of the Andean fold-thrust belt, Bolivia, and the origin of the Central Andean Plateau. Tectonophysics 399:15–37

Mendez V, Villar LM (1979) Los filones ultrabásicos del Río Piedras, Sierras Subandinas de Salta y Jujuy. VII Congreso Geológico Argentino, Actas 2:16–29

Menegatti N (2001) El complejo alcalino Sierra de Rangel, provincia de Salta, Argentina. PhD. thesis, Universidad Nacional de Salta, Argentina

Mon R (1993) Influencia de la orogénesis Oclóyica (Ordovícico-Silúrico) en la segmentación andina en el Noroeste Argentino. 12 Congreso Geológico Argentino 3:65–71

Moreno JA (1970) Estratigrafía y paleogeografía del Cretácico superior de la Cuenca del Noroeste Argentino, con especial mención de los Subgrupos Balbuena y Santa Bárbara. Rev Asoc Geol Argentina XXV 1:9–44

Morimoto N, Fabries J, Ferguson AK, Ginzburg IV, Ross M, Seifert FA, Zussman J, Aoki K, Gottardi G (1988) Nomenclature of pyroxenes. Am Mineral 73:1123–1133

Mpodoziz C, Ramos VA (1990) The Andes of Chile and Argentina. In: Ericksen GE, Cañas Pinochet MT, Reinemuf JA (eds) Geology of the Andes and its relation to hydrocarbon and mineral resources. Circumpacific Council for Energy and Mineral Resources, Earth Sci Series 11: 59–90

Nakamura R, Coombs DS (1973) Clinopyroxene in the Tawhiroko tholeiitic dolerite at Moeraki, northeastern Otago, New Zealand. Contrib Mineral Petrol 42:213–228

Nedli Zs, Tóth TM (2007) Origin and geodynamic significance of Upper Cretaceous lamprophyres from the Villany Mts. (S Hungary). Mineral Petrol 90:73–107

Ngounouno I, Dérruelle B, Montigny R, Demaiffe D (2005) Petrology and geochemestry of monchiquites from Tchircotché (Garoua rift, north Cameroon, Central Africa). Mineral Petrol 83:167–190

Omarini RH, Salfity JA, Linares E, Viramonte JG, Gorustovich AS (1989) Petrología geoquímica de un filón lamprofírico en el Subgrupo Pirgua (Alemanía-Salta). Revista del Instituto de Geología y Minería, Universidad Nacional de Jujuy, 7

Omarini RH, Sureda RJ, Götze HJ, Seilacher A, Plüger F (1999) The Puncoviscana folded belt: a testimony of Late Proterozoic Rodinia fragmentation and the collisional pre-Gondwanic episodes. Int J Earth Sci 88:76–97

Omarini RH, Sureda RJ, Escayola MP, Pimentel M, Matteini M (2005) Datos preliminares (Sm-Nd) en lavas de la fm. Puncoviscana, Provincias de Salta y Jujuy, República Argentina. XVI Congreso Geológico Argentino, La Plata 1:181–184

Phillips WJ (1968) The crystallization of the teschenite from the Lugar Sill, Ayrshire. Geol Mag 105:23–34

Philpotts AR (1972) Density, surface tension and viscosity of the immiscible phase in a basic alkaline magma. Lithos 5:1–18

Philpotts AR (1976) Silicate liquid immiscibility: its probable extent and petrogenetic significance. Am J Sci 276:1147–1177

Ramos VA (2000) The southern Central Andes. In: Cordani UG, Milani EJ, Thomaz Filho A, Campos DA (eds) Tectonic evolution of South America. 31 st International Geological Congress, Río de Janeiro, Brazil, pp. 560–604

Reyes FC, Salfity JA (1973) Consideraciones sobre la estratigrafía del Cretácico (Subgrupo Pirgua) del norte Argentino. VI Congreso Geológico Argentino, Buenos Aires, Actas 1:205–223

Rieder M, Cavazzini G, D'Yaconov Y, Frank-Kamenetskii V, Gottardi G, Guggenhein S, Koval P, Muller G, Neiva A, Radoslovich E, Robert JL, Sassi F, Takeda H, Weiss Z, Wones D (1998) Nomenclature of mica. Can Mineral 36:905–912

Rock NMS (1979) Petrology and origin of the type monchiquites and associated lamprophyres of the Serra de Monchique, Portugal. Trans R Soc Edinburgh 70:149–170

Rock NMS (1987) The nature and origin of lamprophyres: an overview. In: Fitton JG, Upton BGJ (eds) Alkaline igneous rocks. Geol Soc London, Spec Publ 30: 191–226

Rock NMS (1991) Lamprophyres. Blackie and Son, Glasgow, pp 43–46

Roden MF, Frey FA, Francis DM (1984) An exemplo of consequent mantle metasomatism in peridotite inclusions in Nunivak Island, Alaska. J Petrology 25:546–577

Rollinson HR (1993) Using geochemical data: evaluation, presentation, interpretation. Longman Group, UK

Romeuf N, Aguirre L, Soler P, Féraud G, Jillard E, Ruffet G (1995) Middle Jurassic volcanism in the Northern and Central Andes. Rev Geol Chile 22:245–259

Rubiolo DG (1992) Zur Geologie, Petrographie und Geochemie der Alkalimagmatite der Sierra de Santa Victoria (E-Kordillere, NW-Argentinien). Clausthaler Geowiss Diss, 41: 145 pp

Rubiolo DG, Schwab K, Sureda R, Viramonte JG (1994) Relación petrogenética entre Sannaitas y Tinguaitas en la comarca de Maiguasi (Departamento de Iruya, província de Salta, Argentina). VII Congreso Geológico Chileno 2:1189–1193

Rubiolo DG, Seggiaro R, Gallardo E, Disalvo A, Sanchez M, Turel A, Ramallo E, Sandruss A, Godeas M (1997) Hoja Geológica 2366-II / 2166-IV. La Quiaca, Provincias de Jujuy y Salta. Instituto de Geología y Recursos Minerales, Servicio Geológico Minero Argentino. Buenos Aires. Boletín: 113 pp

Rubiolo DG, Gallardo E, Disalvo A, Sanchez M, Turel A, Seggiaro R, Ramallo E, Sandruss A, Godeas M, Gonzalés O (2003) Hoja Geológica 2366-II / 2166-IV La Quiaca, Provincias de Jujuy y Salta. Instituto de Geología y Recursos Minerales, Servicio Geológico Minero Argentino. Buenos Aires. Boletín 246: 123 pp

Russo A, Rodrigo LA (1965) Estratigrafía y paleogeografía del Grupo Puca em Bolívia. Boletín del Instituto Boliviano del Petróleo 5 (34):5–53

Salfity JA, Marquillas RA (1981) Las unidades estratigráficas cretácicas del Norte de la República Argentina. In: Volkheimer W, Musacchio E (eds) Cuencas sedimentarias del Jurásico y Cretácico de América del Sur. Comité del Jurásico y Cretácico, 1: 303–317

Salfity JA (1982) Evolución paleogeográfica del Grupo Salta (Cretácico-Eogénico), Argentina. V Congreso Latinoamericano de Geología, Buenos Aires, 1: 11–26

Scheuber E, Bogdanic T, Lensen A, Reutter KJ (1994) Tectonic development of north Chilean Andes in relation to plate convergence and magmatism since the Jurassic. In: Reutter KJ, Scheuber E, Wigger PJ (eds) Tectonics of the Southern Central Andes. Springer, Berlin, pp 121–139

Schultz F, Lehmann B, Tawackoli S, Rosseling R, Belyatsky B, Dulski P (2004) Carbonatite diversity in the Central Andes: the Ayopaya alkaline province, Bolivia. Contrib Mineral Petrol 148:391–408

Seggiaro RE, Gallardo EF (2002) Low Paleozoic extensional tectonic evidence in the Quebrada de Humahuaca: Cordillera Oriental, Argentina. E Simposio Internacional de Geodinamica Andina, V1 pp 593, Toulousse, France

Sempere T, Carlier G, Soler P, Fornari M, Carlotto V, Jacay J, Arispe O, Néraudeau D, Cárdenas J, Rosas S, Jimenéz N (2002) Late Permian-Middle Jurassic lithospheric thinning in Peru and Bolivia, and its bearing on Andean-age tectonics. Tectonophysics 345:153–181

Smith RE (1967) Segregation vesicles in basaltic lava. Am J Sci 265:696–713

Strong DF, Harris A (1974) The petrology of Mesozoic alkaline intrusives of Central Newfoundland. Can J Earth Sci 11:1208–1219

Sun S, McDonough WF (1989) Chemical and isotopic systematic of ocean basalts: implication for mantle, composition and processes. In: Sounders AD, Norry MJ (eds) Magmatism in ocean basins. J Geol Soc London Spec Publ 42: 313–345

Szabó CS, Kubovics I, Molnár ZS (1993) Alkaline lamprophyre and related dyke rocks in NE Transdanubian, Hungary: The Alcsút-doboz-2 (AD-2) borehole. Mineral Petrol 47:127–148

Thompson RN (1982) Magmatism of the British Tertiary volcanic province. Scott J Geol 18:49–107

Toselli AJ, Aceñolaza FG (1984) Presencia de eruptivas basálticas en los afloramientos de la Formación Puncoviscana, en Coraya, Departamento Humahuaca, Jujuy. Rev Asoc Geol Argentina 39 (1–2):158–159

Turner JCM (1960) Estratigrafía de la Sierra de Santa Victoria y adyacencias. Academia Nacional de Ciencias, Córdoba, Boletín 41:163–196

Turner JCM, Mendez V (1975) Geología del Sector Oriental de los Departamentos de Santa Victoria e Iruya, Provincia de Salta, Republica Argentina. Córdoba LI: 11–24.

Ulrych J, Dostal J, Hegner E, Balogh K, Ackerman L (2008) Late Cretaceous to Paleocene melilitic rocks of the Ohre/Eger Rift in northern Bohemia, Czech Republic: insights into the initial stages of continental rifting. Lithos 101:141–161

Upton BGJ, Wadsworth WJ (1971) Rhyodacite glass in Reunion basalt. Mineral Mag 38:152–159

Vargas Gil JR (1965) Contribución al conocimiento geológico de los alrededores de Tupiza (República de Bolivia). Unpublished Thesis, Facultad de Ciencias Naturales, Universidad de La Plata, 93 pp

Vichi G, Stoppa F, Wall F (2005) The carbonate fraction in the carbonatitic Italian lamprophyres. Lithos 85:154–170

Viramonte JG, Kay SM, Becchio R, Escayola M, Novitski I (1999) Cretaceous rift related magmatism in central-western South America. J South Amer Earth Sci 12:109–121

Wass SY (1979) Multiple origins of clinopyroxes in alkali basaltic rocks. Lithos 12:115–132

Winchester JA, Floyd PA (1977) Geochemical discrimination of different magma series and their differentiation products using immobile elements. Chem Geol 20:325–343

Xu XW, Zhang BL, Qin KZ, Mao Q, Cai XP (2007) Origin of lamprophyres by the mixing of basic and alkaline melts in magma chamber in Beiya area, western Yunnan, China. Lithos 99:339–362

Zappettini EO (1998) El Complejo Alcalino Santa Julia, provincial de Jujuy, República Argentina. X Congreso Latinoamericano de Geología y VI Congreso Nacional de Geología Económica, Buenos Aires 2: 289–294

Zonenshayn LP, Savotin LA, Sedov AP (1984) Global paleogeodynamic reconstructions for the last 160 million years. Geotectonics 18:181–195